AGU PUBLICATIONS

JGR

Journal of Geophysical Research: Atmospheres

RESEARCH ARTICLE
10.1002/2013JD021040

Key Points:
- First latitudinal variation of aerosols from IGP to Himalayas
- First comprehensive calculations of heating rate
- Large gradient in heating rates seen from IGP to Himalayas

Correspondence to:
U. C. Dumka,
dumka@aries.res.in;
snt@iitk.ac.in

Citation:
Dumka, U. C., S. N. Tripathi, A. Misra, D. M. Giles, T. F. Eck, R. Sagar, and B. N. Holben (2014), Latitudinal variation of aerosol properties from Indo-Gangetic Plain to central Himalayan foothills during TIGERZ campaign, *J. Geophys. Res. Atmos.*, *119*, 4750–4769, doi:10.1002/2013JD021040.

Received 16 OCT 2013
Accepted 20 MAR 2014
Accepted article online 30 MAR 2014
Published online 23 APR 2014

Latitudinal variation of aerosol properties from Indo-Gangetic Plain to central Himalayan foothills during TIGERZ campaign

U. C. Dumka[1], S. N. Tripathi[2], Amit Misra[2], D. M. Giles[3,4], T. F. Eck[5,4], Ram Sagar[1], and B. N. Holben[4]

[1]Aryabhatta Research Institute of Observational Sciences, Nainital, India, [2]Department of Civil Engineering, Indian Institute of Technology, Kanpur, India, [3]Sigma Space Corporation, Lanham, Maryland, USA, [4]NASA Goddard Space Flight Center, Greenbelt, Maryland, USA, [5]Universities Space Research Association, Columbia, Maryland, USA

Abstract As part of TIGERZ campaign, latitudinal variation of aerosol optical properties was analyzed over Indo-Gangetic Plains (IGP) to central Himalayas during premonsoon of 2008 and 2009. Measurements of aerosol optical depth (AOD) were performed using Aerosol Robotic Network Sun photometer at four sites with different aerosol environments. The AOD increases from Nainital located in central Himalayas to Kanpur located in IGP region. Further, aerosol size varies spatially with dominance of coarse-mode aerosols at Kanpur compared to fine-mode aerosols dominated at Nainital. Spectral variation of single-scattering albedo suggests that during premonsoon, dust is the dominant species in the IGP with exception of Pantnagar, where absorbing aerosols are dominant. The optical properties of aerosols are calculated, and shortwave clear-sky aerosol radiative forcing (ARF) is estimated. An insignificant difference is found in columnar ARF and columnar heating rate (HR) when vertical profiles of aerosols are included in radiative transfer models. Over Nainital, average ARF is estimated to be −7.61, −45.75, and 38.14 W m^{-2} at top of atmosphere (TOA), surface (SUR), and in the atmosphere (ATM), respectively. Average ARF is less negative at Kanpur compared to Pantnagar and Bareilly with values −17.63, −73.06, and 55.43 W m^{-2} at TOA, SUR, and ATM, respectively. ARF shows positive gradient from the highlands to the IGP sites; larger TOA and SUR cooling were observed at the three sites compared to the highland site. This translates into large columnar HR with estimated average values as 1.07, 1.41, 1.58, and 1.56 K d^{-1} for Nainital, Pantnagar, Bareilly, and Kanpur, respectively.

1. Introduction

Atmospheric aerosols significantly influence the energy balance of Earth's atmosphere and surface, thus modulating the climate and the hydrological cycle [*Forster et al*., 2007]. Although our scientific knowledge of atmospheric aerosols has improved by inclusion of ground-based satellite remote sensing and in situ measurements, the associated uncertainties in the estimation of aerosol radiative forcing are still larger than those for greenhouse gases [*Forster et al*., 2007]. Therefore, it is very important to improve the aerosol characterization on the regional scale with high spatial and temporal resolutions [*Dey and Di Girolamo*, 2010] to account for the large spatial heterogeneity in aerosol properties. Recent ground-based and satellite observations have shown the high aerosol loadings in the Indo-Gangetic Plain (IGP) in north India [*Girolamo et al*., 2004; *Tripathi et al*., 2005; *Jethva et al*., 2005; *Dumka et al*., 2008]. The premonsoon (April to June) and monsoon months are dominated by coarse-mode mineral dust from Thar Desert region and alluvial dust from agriculture fields [*Giles et al*., 2011]. More recently, from aircraft experiments over the region, *Jaidevi et al*. [2011] have reported the observed aerosol optical depth (AOD) (at 0.87 μm) from surface to 3.3 km altitude to be 0.11 during a sortie over rural area around Kanpur. However, concurrent Aerosol Robotic Network (AERONET) retrieved AOD at Kanpur was 0.22 suggesting 50% of AOD to be contributed from aerosols (mostly dust) above 4 km. Based on an altitude variation of aerosol optical and physical properties, *Dumka et al*. [2011] have shown that during the winter season aerosol below 1 km contributes the major fraction of AOD over the central Himalayan region.

Using the aircraft measurements over Kanpur during the winter of the year 2004, *Tripathi et al*. [2005] have shown an enhanced layer of black carbon (BC) aerosols at an altitude of ~0.9 km which gets convected up to a higher altitude (>1.2 km) during the summer [*Tripathi et al*., 2007]. The dominance of absorbing aerosol (such as BC and dust) below 3.3 km over IGP and the foothills of the Himalayas have been studied by aircraft and

satellite-based measurements [*Gautam et al*., 2010; *Jaidevi et al*., 2011; *Srivastava et al*., 2012]. Based on CALIPSO (Cloud-Aerosol Lidar and Infrared Pathfinder Satellite Observations) attenuated backscatter profile, *Jaidevi et al*. [2011] show that aerosols above 4–6 km are possibly due to transport of mineral dust and persistence of elevated aerosol layer (EAL). Based on Micro-Pulse Lidar Network measurements over Kanpur, *Misra et al*. [2012] have reported the existence of EAL at altitudes of 2–4 km during April to May whereas CALIPSO profile indicates the EAL top extending to ~5 km over the northern Indian region [*Gautam et al*., 2009b, 2010]. The EAL, possibly containing a high concentration of absorbing aerosols, could lead to "elevated heat pump (EHP)" scenario with consequent impacts on monsoon [*Lau et al*., 2006]. It is also linked to the dust concentration around the Tibetan Plateau during premonsoon [*Lau et al*., 2006; *Gautam et al*., 2009b].

Recently, *Gautam et al*. [2010] estimated the heating rate (HR) profiles over the entire IGP region (25°N–27°N, 78°E–82°E) using satellite (CALIPSO, CERES) and AERONET Sun photometer observations. They showed that aerosol loading over the IGP region is dominated by dust and is vertically extended to high altitude (~5 km) with enhanced heating in the middle troposphere (5–6 km). *Kuhlmann and Quaas* [2010] analyzed CALIPSO observations and calculated the HR profiles during the premonsoon seasons in three consecutive years (2006–2008) over the region 20°N to 50°N and 60°E to 120°E, covering a vast region including Tibetan Plateau, Taklamakan Desert, Ganges and Indus Plains, and Arabian Sea. All these studies either focused over only a part of IGP or used satellite data which has considerable uncertainty, and the Gangetic-Himalayan (GH) region is not yet covered.

The Himalayan region includes some part of the northern India and merges with the densely populated IGP region with high pollution levels. The aerosols in the IGP can be lifted to higher altitudes and may impact the radiation budget of the climatically sensitive region of Himalayas. The simultaneous observations of aerosol properties are sparsely characterized over the IGP and Gangetic-Himalayan (GH) region. Toward achieving the simultaneous aerosol data set from central IGP through foothills, the TIGERZ program [*Giles et al*., 2011] was conducted during the premonsoon (April to June) of 2008 and 2009 in the northern India. The objectives of the TIGERZ program include spatial and temporal characterization of columnar aerosol optical, microphysical, and absorption properties during the premonsoon season in the IGP and GH regions. Recently, *Kuhlmann and Quaas* [2010] had used aerosol data from CALIPSO to evaluate the heating rates and *Gautam et al*. [2010] used the higher accuracy Level 2 AERONET and satellite data from a single-station Kanpur to evaluate the aerosol radiative properties over the whole IGP region. Even though the surface measurements cannot provide the understanding over a large region like IGP, they do have higher accuracy. On the other hand, satellite-based computations, though limited by accuracy, are more suitable for regional studies. Further, extending single-station data to represent aerosol properties over a large region [e.g., by *Gautam et al*., 2010] will not reveal the heterogeneity in the aerosol properties prevalent over the region [*Srivastava et al*., 2011, 2012]. In the present study, we have therefore made use of multiple station data from AERONET, in conjunction with the CALIPSO-derived aerosol profiles, to evaluate the heterogeneity and latitudinal gradient in the aerosol properties over the IGP. Thus, the present study builds up on the similar studies previously made over the region and constitutes the next step in providing more accurate assessment of aerosol properties and radiative forcing over the IGP. In this paper, we present simultaneous measurements of aerosol properties (e.g., AOD, aerosol size distribution, single-scattering albedo (SSA), aerosols absorption optical depth (AAOD), and optical depth fractions of fine and coarse-mode aerosols) made at four sites situated in the latitude range between 26° and 30°N (a latitudinal span of ~4°) in the IGP. In addition, a comprehensive calculation of aerosol radiative forcing (ARF) and HR profiles over IGP to central Himalayan region is done using CALIPSO-derived extinction profiles and high-quality AERONET level 2 data. The climate implications of the results are also discussed.

2. Study Regions and Instrumentation

2.1. Regions of Study

The present study is focused on four AERONET sites in IGP affected by high aerosol loading emitted from local and regional sources. These sites are Kanpur (26.5°N, 80.2°E, 142 m above mean sea level, (amsl)), Bareilly (28.4°N, 79.4°E, 180 m amsl) in the IGP, Pantnagar (29.1°N, 79.5°E, 230 m amsl) in the Himalayan foothills, and Nainital (29.4°N, 79.5°E, 1958 m amsl), a highland station in the central Himalayas. The highland station is located on a mountaintop called Manora Peak in the hilly terrain of central Himalayas [*Dumka et al*., 2011]. About ~300 km to the west lie densely populated regions including the Indian capital (New Delhi), and the southern region includes heavily populated IGP [*Dumka et al*., 2008].

The AERONET site at Pantnagar is located in the premises of the College of Basic Sciences and Humanities, Govind Ballabh Pant University of Agriculture and Technology. The site has a perimeter of 28.52 km and a large area of about 16,000 acres, which is used primarily for agricultural research. Pantnagar is considered as a rural/semiurban land mass in the foothills of Himalayas. This site is surrounded by regions of small-scale industrial activity, and there are some automobile movements inside the university campus. The industrial activity is a source of occasional strong smoke emissions observed at Pantnagar.

Bareilly is one of the important cities in the north Indian state of Uttar Pradesh and is situated on the banks of the Ramganga River. It is an important commercial center in the northern India with several small- and medium-sized industries. The Bareilly AERONET site lies entirely in the IGP region. The lower Himalayan range is ~100 km away toward the north.

Kanpur (located in IGP region) is one of the major industrial cities in north India with a population of nearly 5 million as per the census report of 2011, and IGP region accommodates ~40% of the Indian population. Kanpur is considered a highly polluted location where anthropogenic and natural aerosols show distinct seasonal and mixing characteristics [*Singh et al*., 2004; *Dey and Tripathi*, 2008; *Giles et al*., 2011]. The aerosol emissions over IGP results from biomass burning in open field (e.g., agricultural waste), domestic fuel in rural settings (e.g., wood and dung cakes), and emissions from fossil fuel sources, such as diesel and kerosene-mixed fuel vehicles and various industrial processes [*Novakov et al*., 2000; *Eck et al*., 2010; *Srivastava et al*., 2011]. During the premonsoon and monsoon seasons, aerosol at Kanpur is strongly influenced by desert dust originating from Thar Desert of India-Pakistan border region and arid regions of farther west [*Jaidevi et al*., 2011] and advecting eastward. Previous studies from Kanpur showed a distinct seasonal pattern of aerosol properties controlled by northeast and summer monsoon [*Dey et al*., 2004; *Jethva et al*., 2005; *Eck et al*., 2010; *Giles et al*., 2011]. The IGP region is generally characterized by northwesterly and westerly to southwesterly winds during the premonsoon season [*Srivastava et al*., 2012].

2.2. AERONET Ground-Based Measurements and Retrievals

As part of TIGERZ program, measurements of aerosol properties were carried out during the premonsoon (April to June) of the year 2008 and 2009 using ground-based AERONET Sun photometer. Only a brief description is given here since a number of studies describe the instrumentation, data acquisition, retrieval algorithms, and calibration procedures as well as the uncertainty of final released products and applied cloud-screening procedures [*Holben et al*., 2001; *Dubovik et al*., 2000; *Smirnov et al*., 2000; *Eck et al*., 2010; *Giles et al*., 2011]. The AERONET measures direct Sun radiance at eight spectral channels (0.34, 0.38, 0.44, 0.50, 0.675, 0.87, 0.94, and 1.02 μm) where 0.94 μm channel is used to estimate columnar water vapor content and the remaining channels are used to retrieve the spectral AODs. The angular distribution of sky radiance is also measured at 0.44, 0.67, 0.87, and 1.02 μm. The measured Sun/sky radiances are used to retrieve the aerosol optical parameters at these four wavelengths by the AERONET inversion code [*Dubovik and King*, 2000]. All the data are available online at the AERONET website (aeronet.gsfc.nasa.gov). The final cloud screened quality assured (Level 2) data product is used in the present study. Here we used both instantaneous and daily-averaged values of AOD at 0.34, 0.38, 0.44, 0.50, 0.675, 0.87, and 1.02 μm wavelengths. We also used the retrieved volume size distribution, single-scattering albedo (SSA), and optical depth fraction of fine- and coarse-mode aerosols at 0.44, 0.67, 0.87, and 1.02 μm available as inversion products from the AERONET [*Dubovik and King*, 2000]. The fine- and coarse-mode AOD was estimated using the Spectral Deconvolution Algorithm (SDA) described elsewhere [*O'Neill et al*., 2001, 2003]. The total uncertainty in the estimated values of τ (λ), varies from ± 0.01 to ± 0.02, which is spectrally dependent with higher errors in the ultraviolet than in the visible range [*Eck et al*., 1999], while the accuracy for the water vapor calculation is 10% [*Smirnov et al*., 2004]. The level-2 SSA almucantar retrieval uncertainty of 0.03 is obtained for $AOD_{440nm} > 0.4$. The retrieval errors for volume size distributions are less than 10% for $0.1 \le r \ge 7$ μm, and it may increase up to 80% for fine ($r \le 0.1$ μm) and coarse ($r \ge 7$ μm) mode particles. However, these errors do not significantly affect the important optical characteristics of aerosols [*Dubovik et al*., 2000].

2.3. MODIS and CALIPSO Satellite-Based Retrievals

The satellite observations used here are from Moderate Resolution Imaging Spectroradiometer (MODIS) aboard the Terra and Aqua satellites. The algorithms used to retrieve MODIS-derived aerosol properties over land are based on dark target and deep blue approaches. The present study uses the retrievals from the dark

Table 1. Aerosol Optical Depth and Single-Scattering Albedo at 0.50 μm

	AOD		SSA	
Sites	AERONET	OPAC	AERONET	OPAC
Nainital (NTL)	0.40 ± 0.02	0.39	0.91	0.81
Pantnagar (PNT)	0.64 ± 0.02	0.63	0.87	0.83
Bareilly (BLR)	0.68 ± 0.02	0.70	0.88	0.82
Kanpur (KNP)	0.61 ± 0.02	0.61	0.89	0.79

target approach only. The uncertainties in MODIS AOD retrieval over land arise from the errors in the surface reflectance, aerosol model type, and instrument calibration [*Levy et al*., 2007]. The overall uncertainty in MODIS-retrieved AOD over land has been estimated as ($\pm 0.05 \pm 0.15\tau$), where τ is the AOD retrieved by MODIS. The evaluation of Collection 5 MODIS-retrieved AOD over land using AERONET observations of AOD shows that MODIS AOD fall within these uncertainties for 72% of the time over land [*Remer et al*., 2008]. Here we have used Collection 5 (C005) level 2 MODIS aerosol products (MOD04 and MYD04, from Terra and Aqua, respectively) at 10 km spatial resolution at all quality assessments (QA; $0 \le \mathrm{QA} < 3$) due to lack of QA = 3 retrievals for 10 km.

The aerosol vertical distribution is obtained from Cloud-Aerosol Lidar with Orthogonal Polarization (CALIOP) onboard the satellite CALIPSO, an instrument which provides global vertically resolved measurements of aerosol and cloud distribution and their optical properties [*Winker et al*., 2007]. The data sets for the premonsoon (April–June) period during the year 2008 and 2009 consist of 204 CALIPSO tracks for each observational site which are used for studying the averaged aerosol profiles. The daytime CALIPSO profiles have lower signal-to-noise ratio compared to the nighttime profiles due to the presence of solar background light. This low value of signal-to-noise ratio may introduce significant errors in the estimation of attenuated backscatter and extinction coefficient profiles. Here we used Level 2 (version 3.01) data that contain elastic backscatter and extinction coefficients at two wavelengths, 0.532 and 1.064 μm.

3. Shortwave Aerosol Radiative Forcing Estimation

The necessary input parameters required for estimation of ARF are AOD, SSA, and asymmetry parameter. Due to lack of aerosol chemical composition measurement for the region under study, standard model from OPAC (Optical Properties of Aerosols and Clouds) [*Hess et al*., 1998] is used to derive the required input parameters by varying aerosol components that contribute to total aerosol over the study region. The OPAC model has been adopted as it allows a wide range of possible aerosol composition in the absence of chemical composition measurements [*Dey and Tripathi*, 2007; *Satheesh et al*., 2010; *Kumar et al*., 2011; *Dumka et al*., 2011, and references cited therein]. Based on observations of near-surface BC mass concentration, AOD and Ångström exponent (α), we have selected the main component of OPAC as water soluble, water insoluble, and soot as the zero-order approximation. A layer of mineral-transported dust is also included at 2 km considering the frequent occurrence of dust storms over the study region during the premonsoon period [*Hegde et al*., 2007; *Gautam et al*., 2009a, 2010; *Kumar et al*., 2011]. Further, details regarding reconstruction of optical properties using OPAC are given elsewhere [*Dey and Tripathi*, 2007; *Satheesh et al*., 2010; *Pathak et al*., 2010; *Kumar et al*., 2011; *Dumka et al*., 2011]. The OPAC-derived AOD spectra agree with the mean values of measured AOD spectra within the measurement error, and OPAC-estimated α value matches with the observed value within 3% [*Dey et al*., 2008; *Dumka et al*., 2011; *Kumar et al*., 2011]. The OPAC simulated and observed AOD and SSA at 0.50 μm is given in Table 1, and a close agreement was found between spectral AOD and SSA from AERONET and OPAC-derived AOD and SSA, ~2%–3% for AOD and ~5%–10% for SSA, respectively.

In order to perform ARF calculations accurately, the atmospheric profiles of temperature, pressure, columnar ozone, water vapor, and surface albedo are required in addition to the aerosol properties. As the observational site is located near the tropical region, the standard tropical atmospheric profiles of temperature and pressure are used along with the surface albedo measured by MODIS onboard Terra and Aqua satellites (8-Day, Level 3 Global 500 m SIN Grid product, MOD09A1 (Terra) and MYD09A1 (Aqua)) at seven wavelength bands centered at 0.645, 0.859, 0.469, 0.555, 1.24, 1.64, and 2.13 μm. The MODIS-derived surface albedo is compared with surface albedo for a mixture of three different surface types, i.e., vegetation, sand, and water as given in Santa Barbara Discrete Ordinate Radiative Transfer (SBDART) [*Ricchiazzi et al*., 1998] following the work given

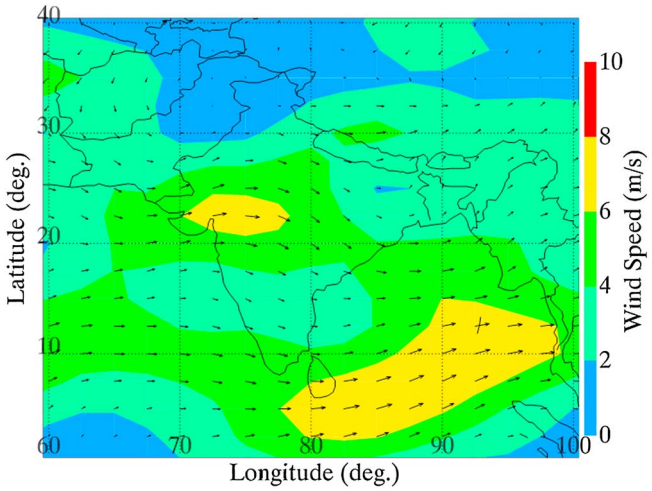

Figure 1. The mean synoptic wind speeds at 850 hpa (based on the NCEP-NCAR reanalysis data) for the period April-May-June of the year 2008 and 2009.

elsewhere [*Ganguly et al.*, 2005; *Pathak et al.*, 2010; *Satheesh et al.*, 2010; *Ramachandran and Kedia*, 2010; *Kedia et al.*, 2010; *Jaidevi et al.*, 2011]. On an average, comparable values of surface albedo are observed within an accuracy of 5% [*Ramachandran and Kedia*, 2010; *Kedia et al.*, 2010; *Satheesh et al.*, 2010; *Pathak et al.*, 2010].

The ARF is the perturbation to the radiative fluxes of Earth's atmosphere system caused by aerosols. The shortwave (SW) ARF calculations are made using SBDART as aerosols mainly interact with incoming solar radiation in SW region (0.25 to 4.0 μm). The SBDART performs plane parallel radiative transfer calculations in clear-sky conditions within the Earth's atmosphere and surface. The AOD, SSA, and asymmetry parameter determined in the wavelength region 0.25 to 4.0 μm are used as an input to SBDART for the radiative transfer calculations. The SW ARF calculations are performed using eight radiation streams at 1 h interval for a range of solar zenith angles, and diurnal averages are calculated. The ARF (ΔF) at TOA and SUR can be written as $\Delta F_{\mathrm{TOA,SUR}} = \mathrm{Flux(net)}_{\mathrm{withaerosolTOA,SUR}} - \mathrm{Flux(net)}_{\mathrm{withoutaerosolTOA,SUR}}$. The difference between ARF at TOA and SUR is defined as the atmospheric radiative forcing (ATM) and can be written as $\Delta F_{\mathrm{ATM}} = \Delta F_{\mathrm{TOA}} - \Delta F_{\mathrm{SUR}}$.

The value of ΔF_{ATM} represents the amount of energy trapped within the atmosphere due to the presence of the aerosols. If the value of ΔF_{ATM} is positive, aerosol leads to a net gain in the radiative flux to the atmosphere leading to a heating, whereas a negative value of ΔF_{ATM} indicates a net loss of radiation flux. The radiative, and hence the climate impact of aerosols, are assessed in terms of atmospheric heating rate (HR). The atmospheric forcing ΔF_{ATM} due to the aerosols in SW region gets converted into heat, and the solar HR is given as $\frac{\partial T}{\partial t} = \frac{g}{C_p}\frac{\Delta F_{\mathrm{ATM}}}{\Delta P}$, where $\partial T/\partial t$ is HR (K d^{-1}), g is the acceleration due to gravity, C_p is the specific heat capacity of air at constant pressure and ΔP is the atmospheric difference between top and bottom boundary of each layer [*Satheesh and Ramanathan*, 2000]. As a large amount of different kinds of aerosols (such as water soluble, BC, sea salt, and mineral dust) are concentrated from surface to ~3 km altitude over the urban, continental, and marine region, ΔP in above equation is considered as 300 hPa, which is equal to the pressure difference between surface and ~3 km altitude.

4. Results and Discussions

4.1. Synoptic Winds

The wind fields at 2.5° × 2.5° spatial resolution and 6-hourly temporal resolution are obtained from NCEP-NCAR (National Centers for Environmental Prediction-National Center for Atmospheric Research) data to understand the influence of synoptic-scale wind features on the spatial and temporal distribution of aerosol properties. The NCEP-NCAR mean synoptic wind speeds at 850 hPa pressure levels over IGP region during study period is shown in Figure 1. The winds are shown with arrows pointing toward wind direction whereas length of arrow gives magnitude of wind speed (m s^{-1}). In general, study region is characterized by westerly to northwesterly winds during the premonsoon seasons which pass through arid/semiarid regions of western India and southwest Asia to bring the dry air mass over the site [*Hegde et al.*, 2007]. During late premonsoon, winds are weak (<5 m s^{-1}) westerlies or westerly to northwesterly, which carry dust from arid regions located in the westernmost part of India and Pakistan (Thar Desert) and Gulf region in the Middle East. Biomass burning aerosols from northwest India and anthropogenic aerosols from IGP affect the aerosol optical properties over the study region [*Lau et al.*, 2006; *Hegde et al.*, 2007; *Srivastava et al.*, 2011; *Jaidevi et al.*, 2011].

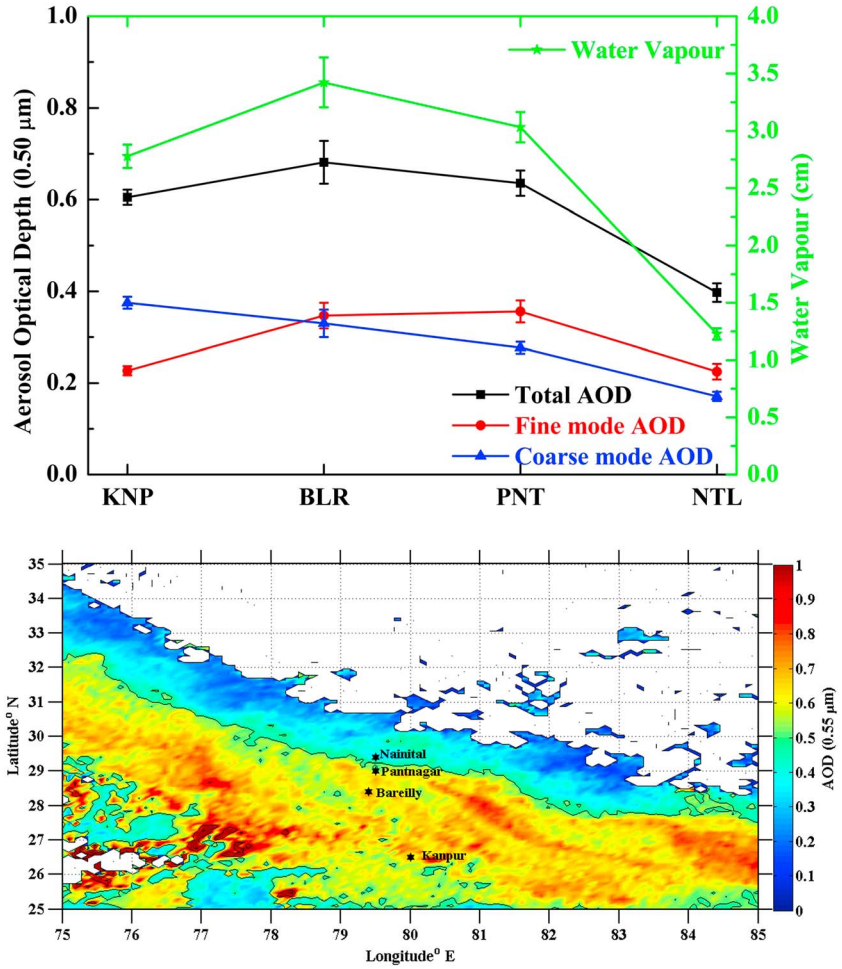

Figure 2. (top) Latitudinal variation of mean total, fine, and coarse-mode aerosol optical depth (AOD) using the ground-based AERONET measurement (primary "*y* axis") and columnar precipitable water vapor in secondary "*y* axis" of same plot. The solid points and vertical bars through them are the mean and standard error in the estimation of mean. There are 46, 49, 40, and 150 days data which are averaged at Nainital, Pantnagar, Bareilly, and Kanpur, respectively, for the estimation of mean during the period under study. (bottom) MODIS level 2 AOD for the period of April to June of years 2008 and 2009. The location of the observational sites is marked in Figure 2 (bottom).

These transported aerosols stagnate over the foothills of Himalayas and then get elevated convectively to higher altitudes due to very high temperature at land surface [*Gautam et al*., 2009b].

4.2. AOD and Size Distribution

The spatial variation of mean AOD_{Total}, $AOD_{Fine\ Mode}$, and $AOD_{Coarse\ Mode}$ at 0.50 μm as a function of latitude is shown in Figure 2 (top), where the precipitable water vapor for the same period is also plotted on the secondary "*y* axis" of the same plot. The solid points correspond to mean AOD value, and vertical bars are standard deviation in the estimation of mean value of total, fine, and coarse-mode AOD and water vapor during premonsoon period. Figure 2 (top) shows the nonuniform spatial variation of AOD with latitude. The observed AOD values for total and fine mode are slightly higher for the corresponding wavelengths over Bareilly than at Kanpur. The AOD values decrease with latitude while moving from Bareilly (IGP site) to Nainital (highland station). In contrast, higher values of fine-mode AOD are observed at Pantnagar. This might have been caused by the rapidly growing industries in the vicinity of the observational site [*Dey et al*., 2004; *Singh et al*., 2004; *Prasad and Singh*, 2007; *Hegde et al*., 2007; *Gautam et al*., 2010; *Giles et al*., 2011; *Kumar et al*., 2011; *Jaidevi et al*., 2011]. In the case of Nainital, a steeper latitudinal gradient (also largely due to altitude) is clearly seen. The mean AOD value at 0.50 μm for Nainital is lower (0.40 ± 0.02; 0.22 ± 0.02; and 0.17 ± 0.01 for total, fine, and coarse-mode aerosols, respectively) compared to the other three sites (Pantnagar; 0.64 ± 0.03;

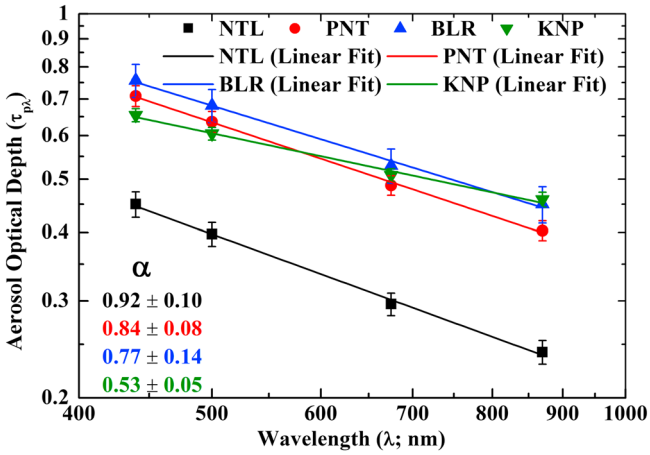

Figure 3. Spectral variation of aerosol optical depth for four AERONET sites. Ångström exponents (α) for all the four sites are also given in the left bottom corner of Figure 3.

0.36 ± 0.02; and 0.28 ± 0.01), (Bareilly; 0.68 ± 0.05; 0.35 ± 0.03; and 0.33 ± 0.03) and (Kanpur; 0.60 ± 0.02; 0.23 ± 0.01; and 0.37 ± 0.01). The lower AOD at Nainital is possibly because the surrounding mountains act as a partial barrier to aerosol transport from the IGP. The observed AOD might be due to local emissions from forest fires, biogenic aerosols, volatile organic carbons, or biomass burning surrounding the observational site [*Kumar et al*., 2011] in addition to long-range transport from west Asia and Indian desert across the IGP [*Hegde et al*., 2007; *Dumka et al*., 2008]. The large variation (0.21 to 0.81) observed in the daily mean AOD at Nainital is important especially in the context of "EHP effect" [*Lau et al*., 2008], which demonstrates the role of elevated layers of absorbing aerosols in the Himalayan region in modification of the Asian monsoon. Accumulation of dust, transported from the arid regions in the west, was also observed over Manora Peak, Nainital, in central Himalayas during premonsoon [*Hegde et al*., 2007; *Dumka et al*., 2008].

Similar type of latitudinal variation of AOD is also observed using the satellite-based measurements. The latitudinal variation of average AOD (MODIS Terra and Aqua platform) over the IGP region during premonsoon period of the year 2008 and 2009 is shown in Figure 2 (bottom). The location of the observational sites is also marked in Figure 2 (bottom). Using ground-based radiometric data during premonsoon period, *Srivastava et al*. [2011, 2012] have studied the various aerosol characteristics over central (Kanpur) and eastern (Gandhi College) parts of IGP. The above mentioned latitudinal variation in AOD is due to actual aerosol loading over the site and is not related to hygroscopic growth of particles. The correlation coefficient between AOD and water vapor content is very poor (R values 0.47, 0.14, 0.23, and 0.27 for Kanpur, Bareilly, Pantnagar, and Nainital, respectively). Similar to AOD, water vapor also shows higher value at Bareilly (3.42 ± 0.22 cm) than at Kanpur (2.78 ± 0.10 cm). The water vapor content decreases while moving from Bareilly to Nainital (Figure 2, top). The average value of water vapor for Nainital and Pantnagar is 1.23 ± 0.02 cm and 3.03 ± 0.13 cm, respectively.

The trajectory cluster analysis clearly shows that the potential aerosol transport pathways originating from the Thar Desert, West or West Asian landmass, or in some cases even from the African region as the West Asian region has vast expansion of the arid/desert areas [*Hegde et al*., 2007; *Dumka et al*., 2010; *Gautam et al*., 2010; *Jaidevi et al*., 2011; *Giles et al*., 2011; *Srivastava et al*., 2011, 2012]. Based on satellite observation, *Prasad and Singh* [2007] have shown that AOD at 0.558 μm increases rapidly from 0.25 to 0.45 over the southern India to 0.60 to 0.75 over IGP. Using multiyear observations of spectral AOD (January 2002 to December 2004), *Dumka et al*. [2008] have reported the role of boundary layer evolution influencing the aerosol characteristics at highland station. The boundary layer plays an important role in transporting aerosols from polluted valley region to higher altitudes. This would result in an increase in the concentration of anthropogenic aerosols at highland site contributing to high AOD over the site during the study period. Using altitude variation of aerosol properties during winter (November–February) of three consecutive years (2005–2007) under fair weather conditions, *Dumka et al*. [2011] have shown that aerosol below 1 km contributes major fraction of AOD. Similar to Nainital, a high value of AOD (0.45) at 0.50 μm is also reported by *Gogoi et al*. [2009] for Dibrugarh (27.3°N, 94.6°E, 111 m amsl located in the northeastern corner of upper Brahmaputra valley) during the premonsoon period.

Besides the general pattern described above, AOD is found to be strongly wavelength dependent as shown in Figure 3. The solid point represents mean AOD, and the vertical bar over the solid point represents standard deviation. The solid line represents the linear least square fit to mean AOD for each site. The AOD spectra is steeper at highland station (implying more abundance of accumulation aerosols) compared to Kanpur, Bareilly, and Pantnagar, where AOD spectra is relatively flat. This suggests a change in aerosol size

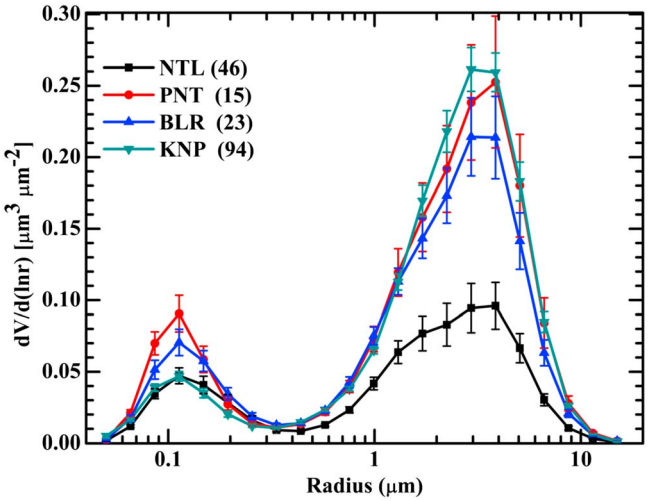

Figure 4. Averaged aerosol volume size distributions over Kanpur, Bareilly, Pantnagar, and Nainital.

spectrum with increased coarse-mode domination. Therefore, size distribution and composition of aerosol particle change are clearly reflected in the AOD spectra (Figure 3). This aspect can be examined by estimating the Ångström parameters (i.e., wavelength exponent (α) and turbidity coefficient (β)). The α is a good indicator of the fraction of accumulation mode aerosols ($r < 1\ \mu m$) to coarse-mode aerosols ($r > 1\ \mu m$). The Ångström parameters in the equation $\tau_{p\lambda} = \beta\lambda^{-\alpha}$ are estimated from the instantaneous measured AOD spectra (by performing a regression analysis between $\tau_{p\lambda}$ and λ (in μm) in log-log scale over the 0.44 to 0.87 μm wavelength range which are then averaged for the individual day). The average values of $\alpha_{0.44-0.87}$ are 0.92 ± 0.10, 0.84 ± 0.08, 0.77 ± 0.14, and 0.53 ± 0.05 for Nainital, Pantnagar, Bareilly, and Kanpur, respectively. The value of α close to 2 indicates small-particle dominance and the value close to zero indicates the dominance of larger aerosols. The highland station shows slightly higher values of α (close to 1) compared to the station in IGP and foothills of Himalayas. These AOD values suggest varying amount of aerosol loading (mostly due to dust) during the period under study. The high values of AOD and low α values represent an increased dominance of wind-driven long-range transport of desert dust [*Hegde et al.*, 2007; *Gautam et al.*, 2009a; *Srivastava et al.*, 2011] as well as regionally generated pollution (e.g., emission from coal-based power plant and brick kilns) as suggested by many investigators [*Singh et al.*, 2004; *Dey et al.*, 2004; *Jethva et al.*, 2005; *Gautam et al.*, 2009a; *Eck et al.*, 2010; *Giles et al.*, 2011].

This can also be examined by estimating aerosol volume size distribution. The average aerosol volume size distribution obtained over the study region for each observational site is depicted in Figure 4, which shows a bimodal structure with a predominant large-particle (coarse) mode besides a (less prominent) small-particle (accumulation/fine) mode. The number of almucantar (46, 15, 23, and 94 for Nainital, Pantnagar, Bareilly, and Kanpur, respectively) is also given in Figure 4. The volume size distribution parameters such as columnar volume concentration (V, $\mu m^3/\mu m^2$), effective radius (R_{eff}, μm), volume median radius (R_v, μm), and geometric standard deviation (σ) for total, fine, and coarse mode are presented in Table 2. The size distribution reveals two distinct modes: fine and coarse-mode aerosols with volume median radii 0.11 μm and 3.0 μm, with higher volume concentration in coarse mode for all the sites. Though the volume concentration is different for these modes, the shape of the distribution is very similar across the four sites. It is characterized by a bimodal log-normal distribution with a prominent peak in coarse mode suggesting a regional dust-dominated environment [*Dey et al.*, 2004; *Singh et al.*, 2004; *Jethva et al.*, 2005].

Based on multiyear measurements of spectral AOD during January 2002 to December 2005, *Dumka et al.* [2009] have also obtained steady bimodal size distributions (number) with a coarse mode centered at ~1.0 μm. The mass and number size distribution of near-surface aerosols measured by Quartz Crystal Microbalance (QCM)

Table 2. Aerosol Volume Size Parameter During the Period Under Study and Unit of Volume Concentration (V; $\mu m^3/\mu m^2$), Effective Radius (R_{eff}; μm), and Volume Median Radius (R_v; μm)

	Total				Fine Mode				Coarse Mode			
Site	V	R_{eff}	R_v	σ	V	R_{eff}	R_v	σ	V	R_{eff}	R_v	σ
NTL	0.22	0.43	1.18	1.36	0.05	0.12	0.14	0.46	0.16	1.92	2.39	0.65
PNT	0.85	1.05	2.49	1.55	0.12	0.14	0.17	0.60	0.79	2.63	3.16	0.65
BLR	0.85	0.80	2.08	1.48	0.16	0.18	0.19	0.53	0.69	2.56	3.21	0.70
KNP	1.10	1.46	3.13	1.64	0.14	0.15	0.18	0.79	1.04	3.11	3.97	0.82

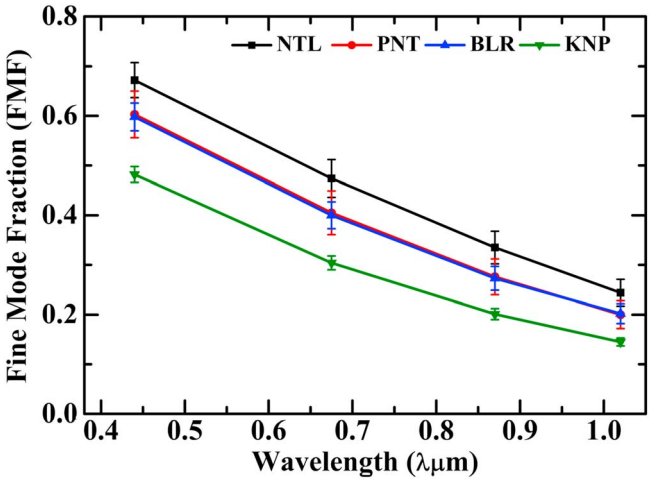

Figure 5. Latitudinal and spectral variations of fine-mode fraction over Kanpur, Bareilly, Pantnagar, and Nainital.

and Optical Particle Counter (OPC) clearly shows enhanced coarse mode during dust activity. Based on OPC measurements at Nainital, *Hegde et al.* [2007] have shown an enhancement in aerosol number concentration for radii above 1.0 μm with an average effective radius of 1.47 μm. This enhancement is 50 and 4 times higher for sizes greater than 5 and 10 μm, respectively compared to 1.0 μm. Measurements over Kanpur were made close to the active source region of dust, whereas those over Nainital are far away from any active source region of dust. Further, Nainital is surrounded by high-altitude mountains of central Himalayas having dense forest with thick vegetation which do not favor any local dust production. Thus, the instruments at Nainital would be sampling transported dust which is of finer size compared to that observed near source region. This volume size distribution clearly implies the dominance of coarse-mode aerosols (mostly dust) over IGP. The concentration of coarse-mode aerosols decreases as we move from Kanpur (IGP site) to the highland site (i.e., Nainital) as shown in Figure 4. The difference in volume concentration of the two modes is higher at Kanpur as compared to the highland station.

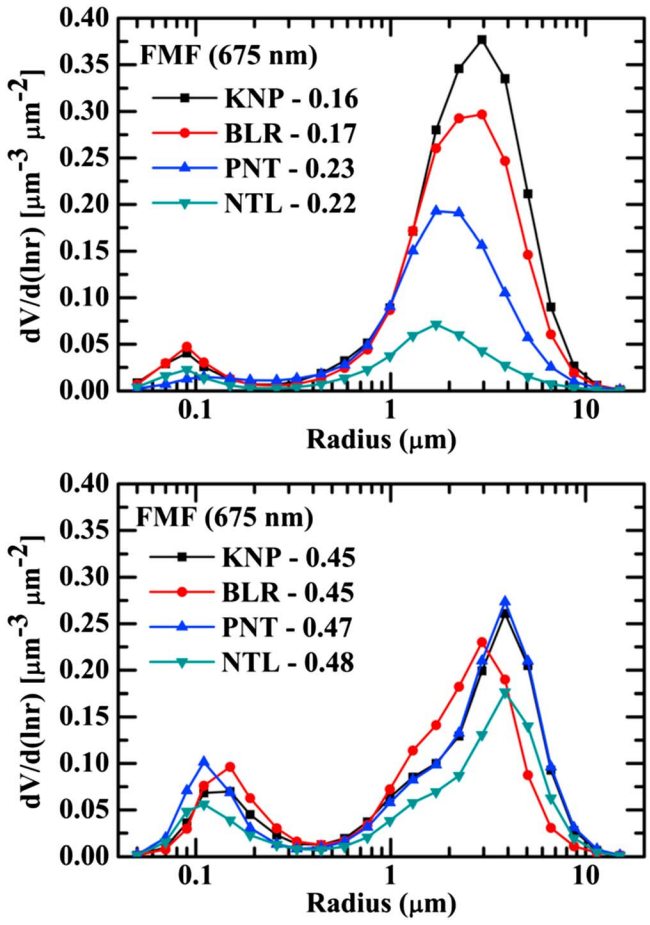

Figure 6. Comparisons of aerosol volume size distribution for all the four AERONET sites for dust-dominated cases (FMF ~0.16) and mixed aerosol cases (FMF ~ 0.45).

4.3. Fine-Mode Fraction

Spectral variation of mean fine-mode fraction (FMF) is shown in Figure 5. In contrast to AOD, FMF (at all the wavelengths) exhibits a uniform spatial variation with latitude, having a steeper latitudinal gradient between Kanpur and highland station. A lower value of FMF (0.40 ± 0.02 at 0.50 μm) was observed at Kanpur compared to highland station (i.e., Nainital, 0.58 ± 0.04) with larger fluctuations as indicated by vertical bars through solid points. Higher value of FMF over highland station represents the dominance of accumulation mode aerosol particles mainly produced from man-made sources in the nearby surrounding regions and transported to the observational site from western region or nearby IGP [*Hegde et al.*, 2007; *Dumka et al.*, 2008]. The lower values of FMF over Kanpur clearly indicate the dominance of higher concentration of coarse-mode aerosols (mostly dust) as indicated by the aerosol volume size distribution (Figure 4). Over IGP, dust activities are found to peak during

Table 3. Aerosol Volume Size Parameter During the Period Under Study for Dust-Dominated Case (FMF = ~0.16) and Mixed Aerosol Case (FMF = ~0.45)[a]

	Total				Fine Mode				Coarse Mode			
Site	V	R_{eff}	R_v	σ	V	R_{eff}	R_v	σ	V	R_{eff}	R_v	σ
Dust-Dominated Aerosols (FMF = ~ 0.16)												
NTL (FMF = 0.22)	0.12	0.43	1.12	1.22	0.02	0.09	0.11	0.55	0.10	1.52	1.81	0.60
PNT (FMF = 0.23)	0.32	0.89	1.64	0.90	0.03	0.14	0.17	0.60	0.29	1.68	2.00	0.59
BLR (FMF = 0.17)	0.49	0.76	1.84	1.03	0.04	0.10	0.11	0.53	0.45	2.02	2.39	0.57
KNP (FMF = 0.16)	0.09	0.95	2.08	0.95	0.04	0.10	0.12	0.60	1.55	2.13	2.54	0.58
Mixed Type Aerosols (FMF = ~ 0.45)												
NTL (FMF = 0.48)	0.28	0.53	1.62	1.36	0.06	0.12	0.13	0.45	0.22	2.37	2.94	0.63
PNT (FMF = 0.47)	0.43	0.50	1.56	1.39	0.09	0.11	0.12	0.40	0.34	2.39	2.95	0.62
BLR (FMF = 0.45)	0.39	0.50	1.28	1.27	0.09	0.14	0.15	0.40	0.31	1.99	2.38	0.58
KNP (FMF = 0.45)	0.41	0.61	1.74	1.28	0.07	0.13	0.14	0.43	0.34	2.32	2.91	0.64

[a]The units of volume concentration (V; $\mu m^3/\mu m^2$), effective radius (R_{eff}; μm), and volume median radius (R_v; μm).

observational period [*Dey et al.*, 2004; *Singh et al.*, 2004]. The larger-size aerosols (dust) result lower FMFs over Kanpur, whereas in mountain regions toward north of Kanpur, central Himalayas exhibit a strong topographical control on dust storms and their transport. During study period, westerly winds were blowing from north Indian plain (Figure 1) causing dust storms. Despite this, observed mean FMF values during the measurement period exhibit strong spectral variations with higher values of FMF at lower wavelengths and vice versa (Figure 5). This clearly implies the persistence of aerosol layer (mostly dust particles) from Kanpur to Pantnagar. However, there are more absorbing aerosols at Pantnagar than at Kanpur, which is also indicated by spectral variation of SSA (see below). Based on FMF value, we classified mainly two types of aerosols prominent in Figure 6, which shows the comparison of aerosol volume size distribution for all the four AERONET sites for dust-dominated cases (FMF = 0.16) and mixed aerosol cases (FMF = 0.45) [*Eck et al.*, 2010]. Volume size distribution parameters for dust-dominated and mixed type aerosols are given in the Table 3.

4.4. Spatial and Spectral Variation of SSA

SSA is the ratio of scattering to total extinction (scattering + absorption) and is given by $SSA = \tau_{scat}/(\tau_{scat} + \tau_{abs})$. SSA characterizes the combined effect of scattering and absorption properties of aerosols. Also, SSA gives the fraction of radiation absorbed by atmospheric aerosols (expressed through 1-SSA). The Sun/sky radiometer retrieves SSA at four different wavelengths 0.44, 0.67, 0.87, and 1.02 μm, respectively. The spectral variation of SSA is the most important parameter after AOD in estimating aerosol radiative effects. The latitudinal and spectral variations of mean SSA values are shown in Figure 7. During premonsoon, the value of SSA at 0.44 μm are 0.91 ± 0.01, 0.86 ± 0.01, 0.87 ± 0.01, and 0.88 ± 0.00 for Nainital, Pantnagar, Bareilly, and Kanpur, respectively while the corresponding values at 1.020 μm are 0.91 ± 0.01, 0.92 ± 0.01, 0.93 ± 0.01, and 0.94 ± 0.00, respectively. The average SSA at all wavelengths was found to be more than 0.86 for all the sites and observed to be relatively lower at Pantnagar than at the other three sites, indicating the dominance of more absorbing type aerosols (such as BC) at Pantnagar in comparison to other sites. The observed SSA in the present study is in general comparable with earlier reported values [*Singh et al.*, 2004; *Dey and Tripathi*, 2008; *Pandithurai et al.*, 2008; *Singh et al.*, 2010; *Giles et al.*, 2011] over IGP during premonsoon. These SSA values are significantly higher than that reported by *Singh et al.* [2010] at New Delhi over IGP.

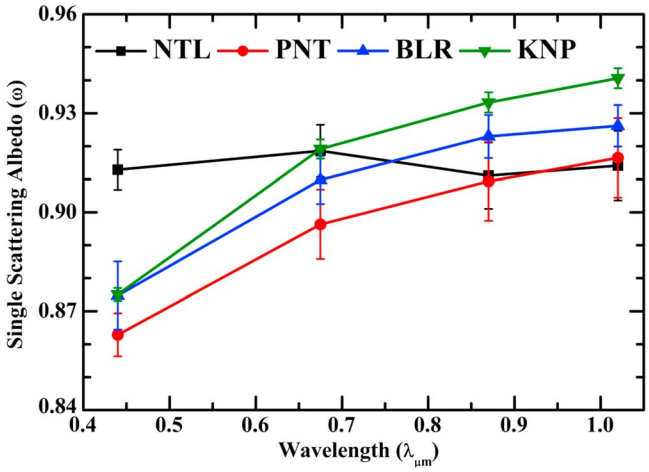

Figure 7. Latitudinal and spectral variations of single-scattering albedo.

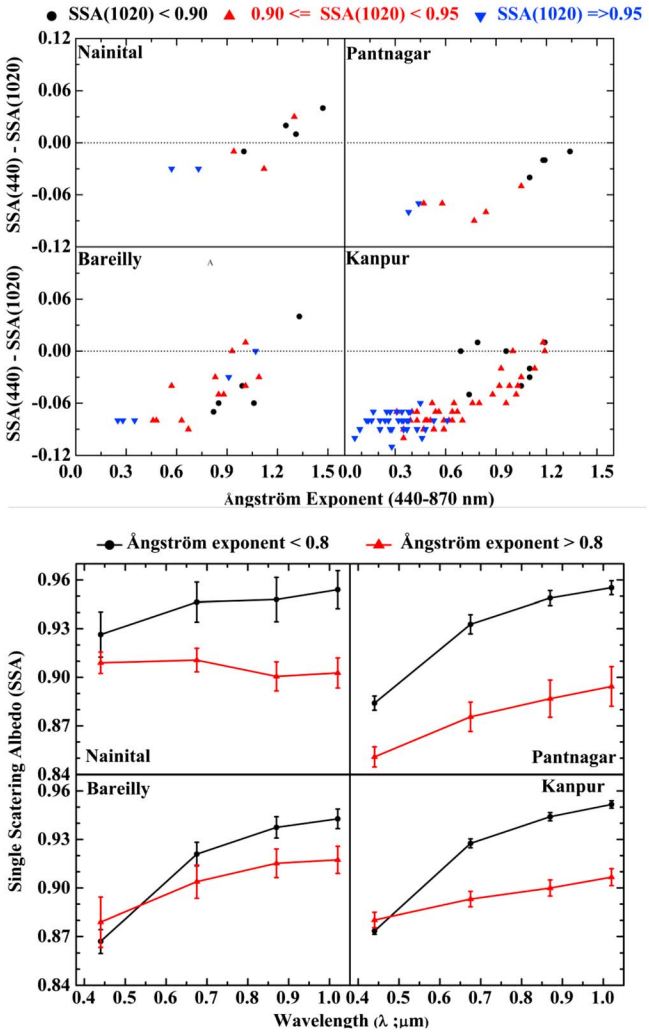

Figure 8. (bottom) Average spectral variation of single-scattering albedo for the periods with significant contribution of coarse (Ångström exponent < 0.8) and fine (Ångström exponent > 0.8) aerosols. (top) Difference of d_{SSA} [= SSA (0.44 μm) − SSA (1.020 μm)] versus Ångström exponent. Different ranges of SSA (1.020 μm) values are presented by different colors and symbols.

On the basis of Sun/sky radiometer measurements, *Pandithurai et al.* [2008] have reported SSA values at New Delhi and SSA at 0.50 μm range between 0.84 and 0.74 from March to June, which indicates the dominance of anthropogenic and desert dust absorbing aerosols. On the basis of near-surface measurements at a nearby station at New Delhi in IGP, *Soni et al.* [2010] found SSA (at 0.55 μm) to be 0.63 ± 0.06. SSA is found to be strongly wavelength dependent with higher value at higher wavelengths (Figure 7) except at Nainital, where SSA has less spectral dependence due to less influence by dust. This could also be attributed to the presence of any other types of absorbing aerosols having less absorption efficiency as highland site (i.e., Nainital) is located in the hilly terrain of central Himalayan region having thick forest. For Pantnagar, Bareilly, and Kanpur, an increase in SSA with wavelength indicates the relative dominance of dust type aerosols as also reported for various episodes of dust storm advection over the IGP region [*Dey et al.*, 2004; *Singh et al.*, 2004; *Pandithurai et al.*, 2008]. A flat spectrum for Nainital shows the dominance of biomass burning aerosols as well as aerosols from fossil fuel combustion. The observed SSA is lowest at Pantnagar, followed by Bareilly, which indicates mostly absorbing aerosols. This is because absorption due to dust aerosols is higher at shorter wavelengths and rapidly decreases at longer wavelengths [*Dey and Tripathi*, 2008; *Bergstrom et al.*, 2007; *Russell et al.* 2010].

In the present study, we have also employed the difference of SSA at 0.44 μm and 1.020 μm (d_{SSA}). This has two advantages. First, the difference will provide a better accuracy than absolute value, since retrieval of spectral dependence is more reliable than that of absolute value. Second, the spectral value of SSA is characterized by a single parameter (i.e., ($SSA_{(0.44\ \mu m)}$–$SSA_{(1.020\ \mu m)}$), d_{SSA}). A negative value of d_{SSA} denotes strong absorption by iron oxide in dust at 0.44 μm, whereas a positive value of d_{SSA} is related to stronger absorption by BC particles at 1.020 μm. This technique should perform adequately for very large SSA (440–1020 nm) differences where dust spectral SSA signatures (e.g., SSA increasing with wavelength for dust) are clear. However, for intermediate cases (e.g., $-0.04 < d_{SSA} < 0$), the aerosol type is much less certain due to the magnitude of the absorption (e.g., SSA440 of 0.96 and SSA1020 of 0.98 may not represent dust) more spectrally neutral strong absorption may represent a possible mixture of dust and BC aerosols [*Giles et al.*, 2011]. The possibility of stronger absorption at 0.44 μm by organic brown carbon could produce a similar SSA signature as dust [*Arola et al.*, 2011]. Dust and organic brown carbon differ in size (and shape) and use of a size parameter (e.g., α) is necessary since d_{SSA} alone cannot absolutely determine the dust aerosol type. Figure 8 (top) shows d_{SSA} versus α (0.44–0.87 μm) for all the four AERONET sites. The data presented in this plot are classified into different ranges of SSA (1.020 μm) in order to indicate the events with different levels of absorption at 1.020 μm.

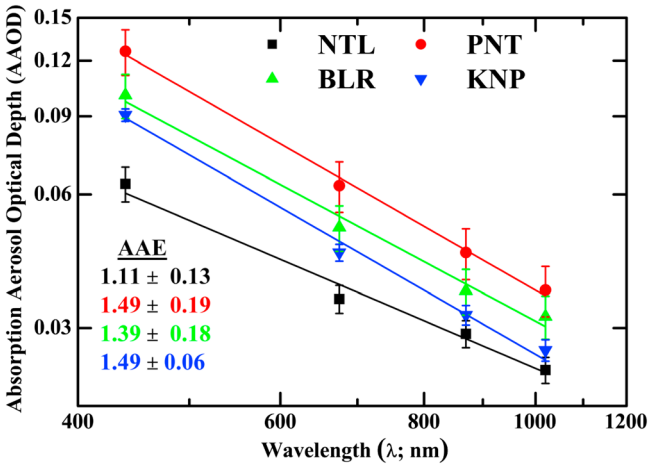

Figure 9. Latitudinal variation of absorption aerosol optical depth over the four AERONET sites. Ångström absorption exponent (AAE) values for all the four sites are also given at the left bottom corner of the Figure 9.

Here we used all the data points in the respective group of SSA (1020). Very few data are available for the three locations Nainital (11 data points), Pantnagar (11 data points), and Bareilly (23 data points) as compared to Kanpur (82 data points). Figure 8 (top) reveals that as α increases from low to high values (indicating a decreasing contribution of coarse-mode dust aerosols and increasing fraction of fine-mode pollution aerosols), spectral SSA gradually changes from strong absorption at 0.44 μm to 1.02 μm. The absorption at 1.02 μm is quite weak as shown in Figure 8 (top) by inverted blue triangles for the case of dust-dominated aerosols.

We selected $\alpha = 0.8$ based on 0.44–0.87 μm as the threshold between coarse and fine aerosols as suggested by *Eck et al.* [2005, 2010]. They showed ~0.8 is about FMF of AOD of 0.5 (i.e., equal parts of fine mode and coarse mode). The SSA during the study period with significant contributions of coarse ($\alpha < 0.8$; case 1) and fine ($\alpha > 0.8$; case 2) are presented in Figure 8 (bottom). This clearly indicates significant differences in spectral variation of SSA for all the four sites under study. The interesting features observed are as follows: (i) strong spectral dependence (i.e., SSA increases with increasing wavelength) was observed in case 1 for all the sites, indicating the relative dominance of dust aerosols over the site and (ii) spectral variation of SSA in case 2 shows similar features with relatively less spectral dependence for Pantnagar, Bareilly, and Kanpur, while for Nainital, flat spectra was observed; however, the magnitude of SSA was found to be relatively low for all the sites.

4.5. Aerosol Type

Following, *Bergstrom et al.* [2007] and *Russell et al.* [2010], the spectral AAODs ($\tau_{abs}\lambda$) were computed from the extinction AOD and SSA as $\tau_{abs}(\lambda) = [1 - \omega_0(\lambda)]^*\tau_{ext}(\lambda)$, where $\omega_0(\lambda)$ is the spectral SSA and $\tau_{ext}(\lambda)$ is the spectral extinction AOD. This is a well-known theoretical equation, which provides information about the absorbing optical properties of aerosols with the term (1-SSA (λ)) representing the fraction of radiation absorbed by atmospheric aerosols. By using the Ångström power law of the form AAOD $(\lambda) = K\lambda^{-AAE}$, where K is particle loading and the Absorption Ångström exponent (AAE) is defined as the negative of the slope of a log-log plot of AAOD versus wavelength. The AAE was computed in a similar fashion as the extinction Ångström exponent using the equation $AAE = -d\ln[\tau_{abs}(\lambda)]/d\ln(\lambda)$. The latitudinal variations of AAOD at four different wavelengths 0.44, 0.675, 0.870, and 1.020 μm, respectively, are shown in Figure 9. It clearly indicates the sharp latitudinal gradient of AAOD with the value of AAOD at all the wavelengths increasing while moving from Kanpur to Pantnagar, except at Nainital where AAOD values are lower than Pantnagar and Bareilly and comparable to Kanpur. This indicates the dominance of absorbing aerosols over Pantnagar. *Bergstrom et al.* [2007] have shown that the fine-mode BC aerosols with relatively constant imaginary refractive index would have AAE equal to 1. However, optically effective and relatively large-size BC aerosols with a constant refractive index can have an AAE of 1.3 [*Bergstrom et al.*, 2007]. *Kirchstetter et al.* [2004] have reported that any deviation in the magnitude of AAE from 1.0 is due to the spectral changes in the imaginary part of refractive index and is related to the composition of aerosol particle. Based on in situ and remote sensing measurements, *Bergstrom et al.* [2007] have shown that AAE values vary from ~1 to 1.2 for pollution aerosols off the east coast of the United States which suggests BC as the principal absorber. For the aerosols dominated by mineral dust with absorption due to iron oxides (strongly absorbing in UV, shorter visible wavelengths), the AAE value would be greater than 1. *Bergstrom et al.* [2007] reported AAE value ~2.3 for long-distance transported Saharan dust. In a recent study over Central Himalayas and its foothills during winter months, *Dumka et al.* [2011] have shown that aerosol absorption over the highland site and its foothills is dominated by mixed type of aerosols. Using multiyear measurement of BC mass concentration at Manora Peak, Nainital in central Himalayas,

Dumka et al. [2010] have shown that BC aerosols observed over Nainital are generally dominated by fossil fuel combustion generated particles. The estimated value of AAE remained mostly around 1 (varying between 0.85 and 1.1). Based on AERONET observations over Kanpur during premonsoon, *Giles et al*. [2011] have reported a mixture of BC and dust aerosols to dominate the absorption. The magnitudes of AAE value for all the stations are also given in the same plot (Figure 9). The AAE value for all the four sites ranges between ~1.1 and 1.5 suggesting mixed type of aerosols to be dominant during premonsoon period. An enhancement of AAE = 1 (value for BC absorption [*Bergstrom et al*., 2007]) is found for all the sites (Figure 9) suggesting that the absorption could be attributed to the presence of mineral dust and biomass burning aerosols over the study region during the premonsoon [*Srivastava et al*., 2011]. *Russell et al*. [2010] and *Giles et al*. [2011] showed that the AAE values vary between ~1.2 and 3.0 for dust, ~0.75 and 1.3 for Urban/Industrial, and ~1.2 and 2.0 for biomass burning aerosols. Using AERONET version 2 almucantar retrievals, *Eck et al*. [2010] showed that the sites dominated by optical mixtures of dust, smoke, and pollution had AAE values between ~1.2 and 1.8 for mixed size particles. Recently, *Soni et al*. [2010] have reported the AAE values at Delhi to be close to unity for near-surface aerosols, indicating that the absorption over the location is due to abundance of BC from fossil fuel burning, whereas large value of AAE ($>$1.0) indicates absorbing aerosols from biomass/biofuel burning. A similar value of AAE is also reported in a recent study over IGP by *Srivastava et al*. [2012]. The AAE value for polluted dust (dominantly dust mixed with anthropogenic particles) and polluted continental type (dominantly anthropogenic aerosols mixed with dust) aerosols were found to be 1.70 and 1.43, respectively, for central IGP (Kanpur) and 1.30 and 1.18, respectively, at eastern IGP (Gandhi College). Using the Sun/sky radiometric observation over IGP during April–June 2009, *Srivastava et al*. [2011] showed that dust aerosol is mostly dominating at Kanpur (AAE = 1.62), compared to that for all the months in the present study (AAE = 1.4) [*Giles et al*., 2012]. Biomass burning aerosols are dominant at Gandhi College (AAE = 1.46) [*Giles et al*., 2012]. A negative gradient of AAE was observed from Kanpur to Gandhi College [*Srivastava et al*., 2011]. In the present study, we have also observed the negative gradient of AAE from Kanpur to Nainital through its foothills.

4.6. Vertical Distribution of Aerosols

Even though the radiometric measurements provide valuable data, the derived information only indicates the column-integrated aerosol loading over the observation site. Vertical profiles of aerosols are important and required for inferring the regional aerosol-induced climate perturbations. Based on CALIPSO measurements and model simulations, *Uno et al*. [2009] showed that the Asian dust originating in China can get transported to great distances around the globe and can be extended to higher altitudes in the upper troposphere, potentially affecting the radiation budget. Aerosol or mineral dust transported over GH region reaches up to the slopes of Himalayas and is further lifted to higher altitudes by strong westerly premonsoon winds combined with enhanced convection and pressure gradient resulting from large topographic differences. Recent study showed mineral dust transported from Thar Desert reaches up to the Central Himalayas and significantly influence the optical, physical, and chemical properties of aerosols at various sites along with southern slopes of Central Himalayas [*Hegde et al*., 2007; *Hyvärinen et al*., 2009; *Ram et al*., 2010; *Gautam et al*., 2011]. In the present study, we utilize the vertical distribution of aerosol backscatter and extinction profiles (during day, night, and total; average of day and night) for Nainital, Bareilly, and Kanpur during premonsoon period of the years 2008 and 2009, averaged over a $1° \times 1°$ box centered over these sites provided by CALIPSO. The plot of extinction profile at 532 nm for the daytime and nighttime along with the total (average of day and nighttime profile) are shown in Figure 10 for Nainital, Bareilly, and Kanpur in top, middle, and bottom panels, respectively. The observed CALIPSO profiles show an elevated layer of aerosols at an altitude of 2 to 3 km above the ground level for Kanpur, while a layer of aerosols was observed at 1.5 km and 3 km above the ground level for highland site Nainital (see Figure 10). Based on the CALIPSO profiles over IGP centered over Kanpur (25°N–27°N, 78°E–82°E), *Gautam et al*. [2010] showed the daytime backscatter peaks ~ 3 km, whereas the nighttime backscatter peak is confined within the boundary layer. The maximum backscatter due to aerosols over the IGP is mostly seen in the 3–4 km altitude and transport of aerosols from Thar Desert to the western IGP and the foothills of Himalayas appear to elevate aerosols to over 4 km.

For Nainital, not much difference between the day and night profiles in the 3–5 km altitude range is observed. In fact, extinction coefficient between 3 to 4 km is identical for the two cases. Thus, the variation between day and night is essentially altitude dependent for different stations. The difference between day and night profiles

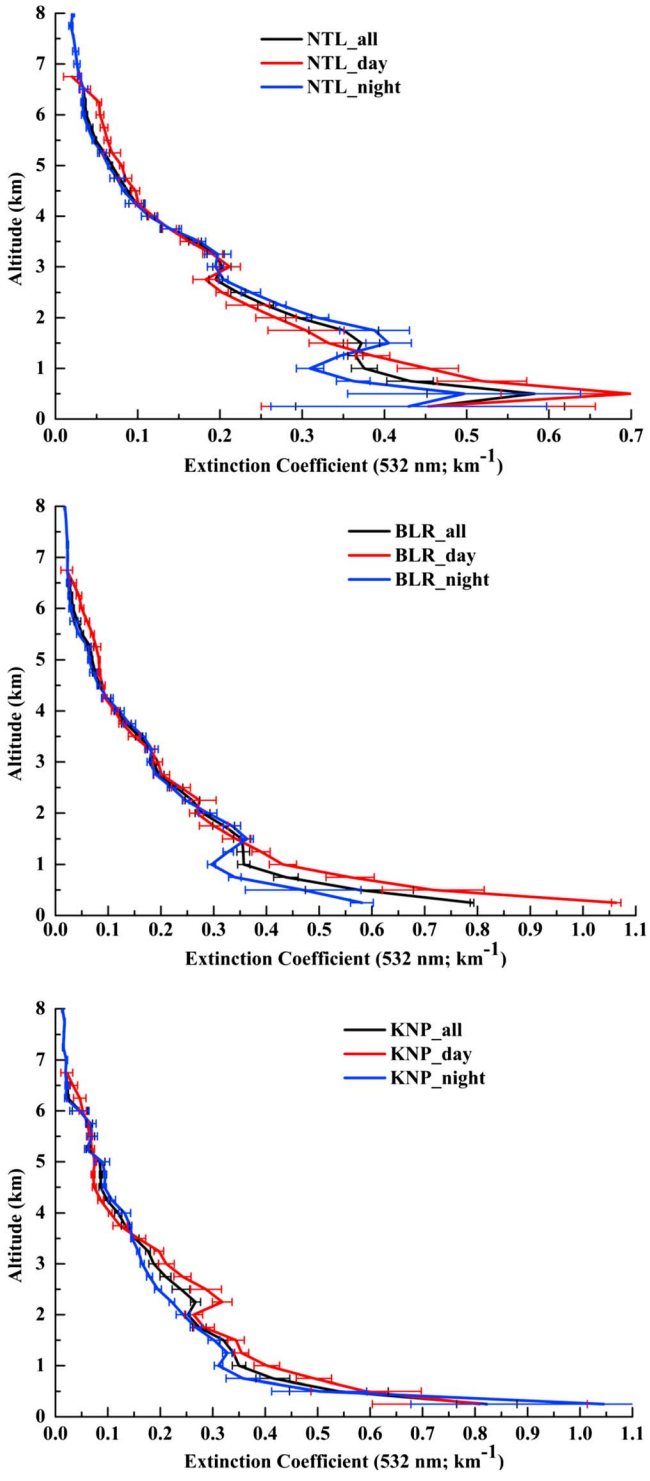

Figure 10. Average vertical distribution of aerosols shown by the space-borne CALIPSO aerosol extinction profiles during the study period averaged over a 1° × 1° box centered over (bottom) Kanpur, (middle) Bareilly, and (top) Nainital, respectively. Black, red, and blue lines represent the total, day, and nighttime profiles, respectively.

is large at Kanpur, and magnitude and sign (i.e., day-night) of difference is altitude dependent. At Kanpur, the nighttime extinction coefficient is higher than daytime extinction coefficient for altitudes greater than ~3.5 km, whereas daytime coefficient is higher than nighttime extinction coefficient for altitudes less than ~3.5 km.

4.7. Aerosol Radiative Forcing, Vertical Profile of ARF, and Heating Rate

The latitudinal variation of shortwave (SW) clear-sky ARF and forcing efficiency (ARF per unit AOD) at TOA, SUR, and in ATM at Nainital, Pantnagar, Bareilly, and Kanpur are shown in Figures 11 (top) and 11 (bottom), respectively. The value of HR is given in parenthesis (Figure 10 top). The TOA and SUR forcing was found to be negative while the ATM forcing was positive. The corresponding TOA, SUR, and ATM forcing were −17.63, −73.06, and 55.43 W m^{-2}, −20.33, −76.52, and 56.19 W m^{-2}, −24.38, −74.59, and 50.22 W m^{-2}, −7.61, −45.75, and 38.14 W m^{-2}, respectively, for Kanpur, Bareilly, Pantnagar, and Nainital. The estimated HR is 1.56, 1.58, 1.41, and 1.07, respectively, for Kanpur, Bareilly, Pantnagar, and Nainital. These values are comparable with values estimated over Kanpur from 2001 to 2005 [*Dey and Tripathi*, 2008]. The estimated ARF and HR for Nainital are comparable to the values reported by *Kumar et al*. [2011] for fire-affected period. The TOA forcing is highest (−24.38 W m^{-2}) for Pantnagar and minimum (−7.6 W m^{-2}) for the highland station Nainital. SUR (−76.52 W m^{-2}) and ATM (56.19 W m^{-2}) forcing are highest for Bareilly. On an average, aerosol-induced SW ARF, during premonsoon months when the transported mineral dust adds to anthropogenic aerosols, is comparable to that for Kanpur, Bareilly, and Pantnagar, while for Nainital the forcing values are comparatively low. The TOA forcing for Kanpur, Bareilly, and Pantnagar are comparable to the value reported by *Jaidevi et al*. [2011] while SUR forcing shows large differences. *Dey and Tripathi* [2008] have also reported the large negative SUR forcing (more than −20 W m^{-2}) with higher values (more than −30 W m^{-2}) during premonsoon months at Kanpur with negative TOA forcing, when the transported

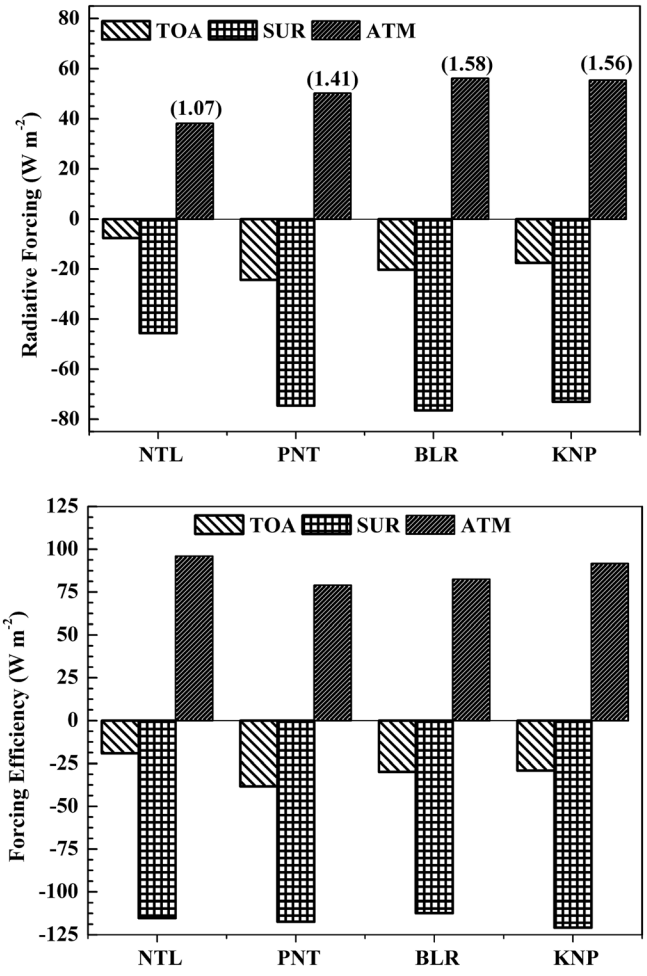

Figure 11. (top) Latitudinal variation of shortwave aerosol radiative forcing at top of the atmosphere (TOA), Surface (SUR), and Atmosphere (ATM) for all the four sites and (bottom) radiative forcing efficiency at TOA, SUR, and ATM. Values of atmospheric heating rate for all sites are given in parentheses.

mineral dusts get mixed with the anthropogenic aerosols. Moreover, *Prasad et al.* [2007] have reported a change in the average SUR forcing by about $-23\ W\ m^{-2}$ and in TOA forcing by about $-11\ W\ m^{-2}$ during the dusty days as compared to the nondusty days during premonsoon season. The large negative SUR and positive ATM forcing over the observation site raise several climatic issues. Figure 11 clearly shows a small latitudinal gradient in ARF. There is a large difference in ARF between SUR and TOA forcing (see Figure 10), suggesting the presence of absorbing aerosols, which is consistent with the relatively low value of SSA (see Figure 7). The ratio (F = SUR/TOA) is an important indicator of the aerosol type. The value of $F > 3$ corresponds to the strong influence of absorbing type aerosols, while values of $F < 2$ indicate scattering type aerosols [*Podgorny et al.*, 2000; *Satheesh and Ramanathan*, 2000]. The F values during the study period over all the observation sites are >3, indicating a large presence of absorbing aerosols. As the absolute values of ARF are strong function of AOD, normalizing the ARF with AOD delineates the aerosol efficiency to attenuate the solar radiation making it an indicator for aerosol type and aerosol absorption efficiency.

The ARF is also dependent on aerosol vertical distribution; lack of information on vertical distribution of aerosols can therefore introduce uncertainty in ARF [*Forster et al.*, 2007]. The dependence of vertical distribution becomes more important in view of aerosol absorption efficiency [*Satheesh et al.*, 2010]. Therefore, we have estimated vertical profile of SW ARF and HR profiles using extinction coefficient profiles obtained from CALIPSO and SBDART by following the method given elsewhere [*Kedia et al.*, 2010; *Ramachandran and Kedia*, 2010]. The SW ARF and HR profiles estimated by including vertical profile of extinction for all the three sites (i.e., Nainital, Bareilly, and Kanpur) are shown in Figures 12 (top) and 12 (bottom), respectively. The total ARF at TOA, SUR, and ATM are also estimated by including the aerosol profiles and are shown in Figure 13. An insignificant difference is found in columnar ARF and HR when vertical profiles of aerosols are included in SBDART (Figure 13; plot for without inclusion of vertical profile aerosols is not shown here). The HR profiles obtained by inclusion of vertical profiles of aerosols are similar to the vertical profiles of aerosols, and HR is found to be higher where elevated aerosol layer exists. The ARF profile obtained for Bareilly and Kanpur are found to be higher as compared to that for Nainital. The HR profile for Kanpur is increasing from surface to ~2 km. During the study period over Kanpur, the peak HR of $1.3\ K\ d^{-1}$ at 1.5 km and $1.45\ K\ d^{-1}$ was observed at 2 km, respectively, for all and day time profiles. The corresponding diurnal TOA and SUR forcing were -0.798 and $-55.839\ W\ m^{-2}$, respectively (see Figure 13). The HR profiles for Kanpur shows a secondary peak HR of $1.10\ K\ d^{-1}$ and $1.20\ K\ d^{-1}$ at 2.8, respectively, for all and day time profiles. These values are quite different in comparison to the values shown in Figure 11. In this estimation, TOA and SUR are estimated with the inclusion of vertical profile of aerosols as input. This suggests that the vertical

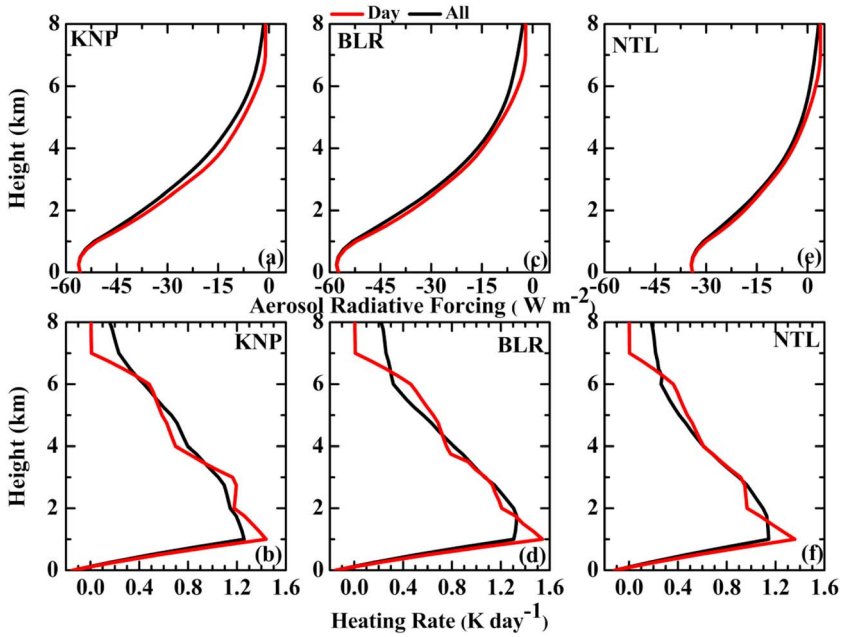

Figure 12. Shortwave aerosol radiative forcing and heating rates as function of altitude obtained with inclusion of aerosol vertical profiles for (left column) Kanpur, (middle column) Bareilly, and (right column) Nainital, respectively.

profile of aerosols affect the TOA and SUR forcing over Kanpur. The HR profile over the central Himalayan site shows similar variation with altitude as Kanpur. The peak values of HR for all and day time profiles were 1.15 and 1.35 K d^{-1}, respectively, from 1 to 2 km. The day time HR profiles show secondary peak HR of 0.9 K d^{-1} at 3 km altitude. Similar to Kanpur and Nainital, Bareilly also shows similar pattern of HR profiles. The peak HR of 1.35 and 1.5 K d^{-1} was observed at 1.5 and 1.0 km, respectively, for all and day time profiles. A closer look at the HR profiles shown in Figure 12 gives more insights into where in the atmosphere actual absorption is happening.

Based on aircraft measurements over Kanpur, *Tripathi et al.* [2007] calculated HR profile from surface to ~1.5 km during premonsoon and reported the HR profile for forenoon (FN) and afternoon (AN) periods of the day.

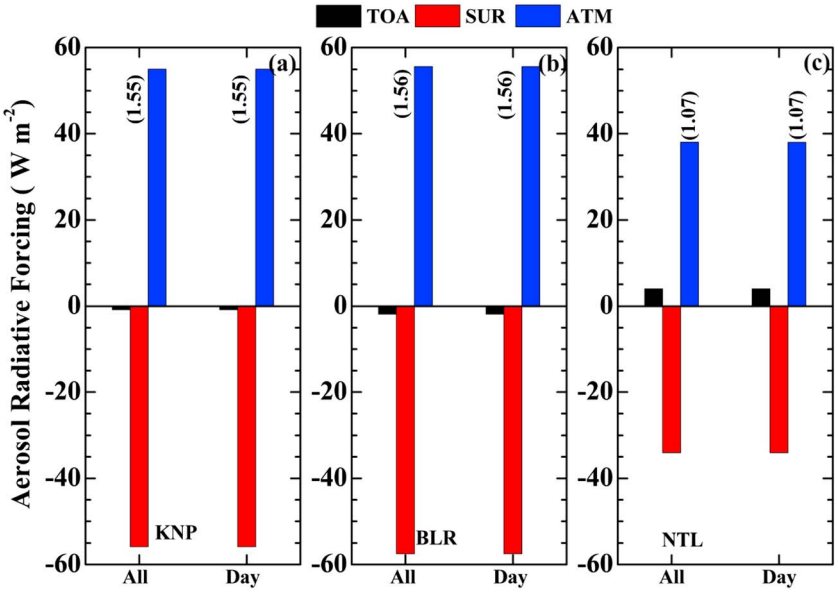

Figure 13. Comparison of shortwave aerosol radiative forcing at the top of the atmosphere, the surface, and in the atmosphere estimated with aerosol vertical profiles. An atmospheric heating rate (K/d) is also given in parentheses.

They found that HR increased with height in AN up to 1.75 K d^{-1}at 1.2 km, whereas the HR profile for FN period increased with height with a first peak of 2.1 K d^{-1} at 0.3 km altitude and a secondary peak of 1.75 K d^{-1} at 1.2 km altitude. This indicates the persistence of high BC mass concentration over the Kanpur region in premonsoon months with significant impact on the regional climate forcing. On the basis of observations over Central Himalayas through its foothills during winter seasons for three consecutive years (2005–2008), *Dumka et al*. [2011] reported the largest heating at the surface level which decreases sharply with increase in altitude. Aerosol-induced atmospheric heating is mainly caused by the dominance of absorbing type aerosols by virtue of the incomplete combustion of fossil fuel combustions and biomass burning activities. Also, the persistence of the high BC mass concentration over the study region would have a significant impact on the regional climate forcing. In recent observations over IGP and the foothills of the Himalayas, *Jaidevi et al*. [2011] have reported that during premonsoon seasons over Kanpur, peak HR of 0.8 K d^{-1} was observed at 2.1 km. In a similar study during the premonsoon season (which increases the proportion of absorbing type aerosols, thereby reducing the SSA value below 0.95) for Bareilly, *Jaidevi et al*. [2011] showed high values (~2.5 K d^{-1}) of HR at 2.1 km altitude, which can lead to boundary layer inversion, thus inhibiting the vertical transport of aerosols [*Tripathi et al*., 2007]. The TOA and SUR forcing over Bareilly were −1.847 and −57.648 W m^{-2}, respectively. This suggests that the HR profiles at Kanpur and Bareilly are highly governed by absorbing type aerosols [*Jaidevi et al*., 2011]. Based on aircraft measurements, *Jaidevi et al*. [2011] evaluated HR profile in the foothills of the Himalayas (Pantnagar) at lower altitudes for the first time and found the maximum value of HR 0.64 K d^{-1}at an altitude of ~2 km. Using CALIPSO lidar backscatter image from southern India to Himalayas, *Gautam et al*. [2009b] showed the vertical extent of aerosols at elevated altitudes (>5 km) piling up against the slopes of the Himalayas and instantaneous radiative heating (due to aerosol absorption) in IGP to be ~6.5 K d^{-1} at 3.5 km, extending up to middle troposphere and resulting in enhanced HR (4.5 – 2 K d^{-1}) in the 4–7 km altitude. Using satellite-based (CALIPSO, CERES) and AERONET data, and one-dimensional radiative transfer model, *Gautam et al*. [2010] estimated the SW HR profile over IGP during premonsoon season for a period of 2 years. Daily average HR over IGP peaked at ~3 km to a value near 2 K d^{-1}, whereas the instantaneous SW HR is found to have a peak value of ~ 6 K d^{-1} at around 3 km altitude. Based on CALIPSO observations, *Kuhlmann and Quaas* [2010] calculated HR during premonsoon seasons in three consecutive years (2006–2008) and found that HR peaks between 2 and 3 km over the Gangetic plains with a peak value of 0.35 K d^{-1}.

The large heterogeneity observed in ARF over IGP and Central Himalayas at short time scale (within a season) has important implications in assessing climate impact. The high value of heating rate up to 2 to 4 km as seen over IGP and the central Himalayan region will have implication for regional climate and Indian monsoon. This value of heating rate can stabilize lower troposphere by strengthening the temperature inversion, thus inhibiting the convection processes. This feedback mechanism will build up more aerosols and will adversely affect the hydrological cycle. Further detailed studies on the impact of enhanced aerosol heating rate during the study period (i.e., premonsoon) and its effect on regional climate are needed.

5. Conclusions

As part of TIGERZ campaign conducted in Indo-Gangetic Plain region to central Himalayas during premonsoon (April–June) period of 2008 and 2009, we have analyzed simultaneous measurements of spectral AOD and AERONET inversion retrievals of column-integrated aerosol optical properties for four different aerosol regimes. The major findings are as follows:

1. Mean AOD during the premonsoon of the years 2008–2009 showed a 0.3 spatial variation with latitude from Kanpur to Nainital. The lowest value (0.40 ± 0.02) for Nainital is due to elevation, and the highest for Pantnagar is due to stagnation of aerosols at the base of the foothills and possible strong local sources.
2. The aerosol volume size distribution computed by inversion of AOD spectra shows bimodal distribution (geometric mean radius is 0.11 μm for fine mode and 3.0 μm for coarse mode). The volume concentration of coarse-mode aerosols increases from Nainital to Kanpur.
3. The SSA of aerosols is found to be strongly wavelength dependent except at Nainital where it is spectrally insensitive. This increasing trend of SSA with wavelength clearly indicates the dominance of aerosol layer with mostly dust particles in premonsoon season.
4. The fine-mode fraction (FMF) indicates the persistence of aerosol layer (mostly dust) from Kanpur to Pantnagar in Himalayan foothills. However, more absorbing fine aerosols are dominant at Pantnagar than at Kanpur.

5. The average Absorption Ångström exponent values over the four sites are 1.11 ± 0.13, 1.49 ± 0.19, 1.39 ± 0.18, and 1.49 ± 0.06 for Nainital, Pantnagar, Bareilly, and Kanpur, respectively, and suggest that mixed type of aerosols are dominant during the study period.
6. The CALIPSO Level 2 (version 3.01) extinction profile shows an elevated layer of aerosols at an altitude of 2 to 3 km above the ground for Kanpur and above 3 km for highland site Nainital.
7. Large TOA, SUR, and ATM forcing was observed at all the stations. The resultant atmospheric forcing exerts significant heating to the atmosphere at all the stations, being 1.07, 1.41, 1.58, and 1.56 $K\,d^{-1}$ for Nainital, Pantnagar, Bareilly, and Kanpur, respectively. These results are largely associated with the measured parameters which are mainly influenced by the synoptic weather condition, emission source, and geography of the sites.
8. An insignificant difference is found in the columnar aerosol radiative forcing and columnar heating rate when vertical profiles of aerosols are included in the radiative transfer model.
9. Large heterogeneity observed in aerosol radiative forcing has important implication in assessing climate impact. The high value of heating rate up to 2 to 4 km over the IGP and central Himalayan region will have the implication for regional climate and Indian monsoon.

Acknowledgments

The authors thank the editor and anonymous reviewers for their valuable comments and suggestions which significantly improved the paper. A part of this work was supported by National Academy of Science and U. S. Agency for International Development. The authors would like to acknowledge Harish Vishwakarma at IIT-Kanpur for field support during TIGERZ. The authors thank the AERONET team for calibrating and maintaining the instrument and processing the data. The NCEP reanalysis data are obtained from http://www.cdc.noaa.gov, and CALIPSO extinction coefficients are obtained from http://www-calipso.larc.nasa.gov/tools/data_avail/.

References

Arola, A., G. Schuster, G. Myhre, S. Kazadzis, S. Dey, and S. N. Tripathi (2011), Inferring absorbing organic carbon content from AERONET data, *Atmos. Chem. Phys.*, *11*, 215–225.

Bergstrom, R. W., P. Pilewskie, P. B. Russell, J. Redemann, T. C. Bond, P. K. Quinn, and B. Sierau (2007), Spectral absorption properties of atmospheric aerosols, *Atmos. Chem. Phys.*, *7*, 5937–5943, doi:10.5194/acp-7-5937-2007.

Dey, S., and L. Di Girolamo (2010), A climatology of aerosol optical and microphysical properties over the Indian subcontinent from 9 years (2000–2008) of Multiangle Imaging SpectroRadiometer (MISR) data, *J. Geophys. Res.*, *115*, D15204, doi:10.1029/2009JD013395.

Dey, S., and S. N. Tripathi (2007), Estimation of aerosol optical properties and radiative effects in the Ganga basin, northern India, during the winter time, *J. Geophys. Res.*, *112*, D03203, doi:10.1029/2006JD007267.

Dey, S., and S. N. Tripathi (2008), Aerosol direct radiative effects over Kanpur in the Indo-Gangetic basin, northern India: Long-term (2001–2005) observations and implications to regional climate, *J. Geophys. Res.*, *113*, D04212, doi:10.1029/2007JD009029.

Dey, S., S. N. Tripathi, and R. P. Singh (2004), Influence of dust storms on the aerosol optical properties over the Indo-Gangetic basin, *J. Geophys. Res.*, *109*, D20211, doi:10.1029/2004JD004924.

Dey, S., S. N. Tripathi, and S. K. Mishra (2008), Probable mixing state of aerosols in the Indo-Gangetic Basin, northern India, *Geophys. Res. Lett.*, *35*, L03808, doi:10.1029/2007GL032622.

Dubovik, O., and M. D. King (2000), A flexible inversion algorithm for retrieval of aerosol optical properties from sun and sky radiance measurements, *J. Geophys. Res.*, *105*, 20,673–20,696, doi:10.1029/2000JD900282.

Dubovik, O., A. Smirnov, B. N. Holben, M. D. King, Y. J. Kaufman, T. F. Eck, and I. Slutsker (2000), Accuracy assessments of aerosol optical properties retrieved from Aerosol Robotic Network (AERONET) Sun and sky radiance measurements, *J. Geophys. Res.*, *105*(D8), 9791–9806, doi:10.1029/2000JD900040.

Dumka, U. C., K. K. Moorthy, S. K. Satheesh, R. Sagar, and P. Pant (2008), Short-period modulations in aerosol optical depths over the central Himalayas: Role of mesoscale processes, *J. Appl. Meteorol. Climatol.*, *47*, 1467–1475, doi:10.1175/2007JAMC16381.

Dumka, U. C., R. Sagar, and P. Pant (2009), Retrieval of columnar aerosol size distributions from spectral attenuation measurements over Central Himalayas, *Aerosol Air Qual. Res.*, *9*, 344–351.

Dumka, U. C., K. K. Moorthy, R. Kumar, P. Hegde, R. Sagar, P. Pant, N. Singh, and S. S. Babu (2010), Characteristics of aerosol black carbon mass concentration over a high altitude location in the Central Himalayas from multi-year measurements, *Atmos. Res.*, *96*, 510–521.

Dumka, U. C., K. K. Moorthy, S. N. Tripathi, P. Hegde, and R. Sagar (2011), Altitude variation of aerosol properties over the Himalayan range inferred from spatial measurements, *J. Atmos. Sol. Terr. Phys.*, *73*, 1747–1761.

Eck, T. F., B. N. Holben, J. S. Reid, O. Dubovik, A. Smirnov, N. T. O'Neill, I. Slutsker, and S. Kinne (1999), Wavelength dependence of the optical depth of biomass burning, urban, and desert dust aerosols, *J. Geophys. Res.*, *104*(D24), 31,333–31,349, doi:10.1029/1999JD900923.

Eck, T. F., et al. (2005), Columnar aerosol optical properties at AERONET sites in central eastern Asia and aerosol transport to the tropical mid-Pacific, *J. Geophys. Res.*, *110*, D06202, doi:10.1029/2004JD005274.

Eck, T. F., et al. (2010), Climatological aspects of the optical properties of fine/coarse mode aerosol mixtures, *J. Geophys. Res.*, *115*, D19205, doi:10.1029/2010JD014002.

Forster, P., et al. (2007), Changes in atmospheric constituents and in radiative forcing, in *Climate Change 2007: The Physical Science Basis. Contribution of Working Group I to the Fourth Assessment Report of the Intergovernmental Panel on Climate Change*, edited by S. Solomon et al., pp. 129–234, Cambridge Univ. Press, Cambridge, U. K., and New York.

Ganguly, D., H. Gadhavi, A. Jayaraman, T. A. Rajesh, and A. Misra (2005), Single scattering albedo of aerosols over the central India: Implications for the regional aerosol radiative forcing, *Geophys. Res. Lett.*, *32*, L18803, doi:10.1029/2005GL023903.

Gautam, R., N. C. Hsu, K.-M. Lau, S.-C. Tsay, and M. Kafatos (2009a), Enhanced pre-monsoon warming over the Himalayan-Gangetic region from 1979 to 2007, *Geophys. Res. Lett.*, *36*, L07704, doi:10.1029/2009GL037641.

Gautam, R., Z. Liu, R. P. Singh, and N. C. Hsu (2009b), Two contrasting dust-dominant periods over India observed from MODIS and CALIPSO data, *Geophys. Res. Lett.*, *36*, L06813, doi:10.1029/2008GL036967.

Gautam, R., N. C. Hsu, and K.-. M. Lau (2010), Premonsoon aerosol characterization and radiative effects over the Indo-Gangetic Plains: Implications for regional climate warming, *J. Geophys. Res.*, *115*, D17208, doi:10.1029/2010JD013819.

Gautam, R., et al. (2011), Accumulation of aerosols over the Indo-Gangetic plains and southern slopes of the Himalayas: Distribution, properties and radiative effects during the 2009 pre-monsoon season, *Atmos. Chem. Phys.*, *11*, 12,841–12,863, doi:10.5194/acp-11-12841-2011.

Giles, D. M., et al. (2011), Aerosol properties over the Indo-Gangetic Plain: A mesoscale perspective from the TIGERZ experiment, *J. Geophys. Res.*, *116*, D18203, doi:10.1029/2011JD015809.

Giles, D. M., B. N. Holben, T. F. Eck, A. Sinyuk, A. Smirnov, I. Slutsker, R. R. Dickerson, A. M. Thompson, and J. S. Schafer (2012), An analysis of AERONET aerosol absorption properties and classifications representative of aerosol source regions, *J. Geophys. Res.*, *117*, D17203, doi:10.1029/2012JD018127.

Girolamo, D. L., T. C. Bond, D. Bramer, D. J. Diner, F. Fettinger, R. A. Kahn, J. V. Martonchik, M. V. Ramana, V. Ramanathan, and P. J. Rasch (2004), Analysis of Multi-angle Imaging Spectroradiometer (MISR) aerosol optical depths over greater India during winter 2001–2004, *Geophys. Res. Lett.*, *31*, L23115, doi:10.1029/2004GL021273.

Gogoi, M. M., K. Krishna Moorthy, S. S. Babu, and P. K. Bhuyan (2009), Climatology of columnar aerosol properties and the influence of synoptic conditions: First-time results from the north-eastern region of India, *J. Geophys. Res.*, *114*, D08202, doi:10.1029/2008JD010765.

Hegde, P., P. Pant, M. Naja, U. C. Dumka, and R. Sagar (2007), South Asian dust episode in June 2006: Aerosol observations in the central Himalayas, *Geophys. Res. Lett.*, *34*, L23802, doi:10.1029/2007GL030692.

Hess, M., P. Koepke, and I. Schult (1998), Optical properties of aerosols and clouds: The software package OPAC, *Bull. Am. Meteorol. Soc.*, *79*, 831–844.

Holben, B. N., et al. (2001), An emerging ground-based aerosol climatology: Aerosol optical depth from AERONET, *J. Gephys. Res.*, *106*, 12,067–12,097.

Hyvärinen, A. P., H. Lihavainen, M. Komppula, V. P. Sharma, V.-M. Kerminen, T. S. Panwar, and Y. Viisanen (2009), Continuous measurements of optical properties of atmospheric aerosols in Mukteshwar, northern India, *J. Geophys. Res.*, *114*, D08207, doi:10.1029/2008JD011489.

Jaidevi, J., S. N. Tripathi, T. Gupta, B. N. Singh, V. Gopalakrishnan, and S. Dey (2011), Observation-based 3-D view of aerosol radiative properties over Indian Continental Tropical Convergence Zone: Implications to regional climate, *Tellus B*, *63*(5), 971–989.

Jethva, H., S. K. Satheesh, and J. Srinivasan (2005), Seasonal variability of aerosols over the Indo-Gangetic basin, *J. Geophys. Res.*, *110*, D21204, doi:10.1029/2005JD005938.

Kedia, S., S. Ramachandran, A. Kumar, and M. M. Sarin (2010), Spatiotemporal gradients in aerosol radiative forcing and heating rate over Bay of Bengal and Arabian Sea derived on the basis of optical, physical, and chemical properties, *J. Geophys. Res.*, *115*, D07205, doi:10.1029/2009JD013136.

Kirchstetter, T. W., T. Novakov, and P. V. Hobbs (2004), Evidence that the spectral dependence of light absorption by aerosols is affected by organic carbon, *J. Geophys. Res.*, *109*, D21208, doi:10.1029/2004JD004999.

Kuhlmann, J., and J. Quaas (2010), How can aerosols affect the Asian summer monsoon?, Assessment during three consecutive pre-monsoon seasons from CALIPSO satellite data, *Atmos. Chem. Phys.*, *10*, 4673–4688, doi:10.5194/acp-10-4673-2010.

Kumar, R., M. Naja, S. K. Satheesh, N. Ojha, H. Joshi, T. Sarangi, P. Pant, U. C. Dumka, P. Hegde, and S. Venkataramani (2011), Influences of the springtime northern Indian biomass burning over the central Himalayas, *J. Geophys. Res.*, *116*, D19302, doi:10.1029/2010JD015509.

Lau, K. M., M. K. Kim, and K. M. Kim (2006), Asian summer monsoon anomalies induced by aerosol direct forcing: The role of the Tibetan Plateau, *Clim. Dyn.*, *26*, 855–864, doi:10.1007/s00382-006-0114-z.

Lau, K. M., et al. (2008), The Joint Aerosol–Monsoon Experiment: A new challenge for monsoon climate research, *Bull. Am. Meteorol. Soc.*, *89*, 369–383.

Levy, R. C., L. A. Remer, S. Mattoo, E. F. Vermote, and Y. J. Kaufman (2007), Second-generation operational algorithm: Retrieval of aerosol properties over land from inversion of Moderate Resolution Imaging Spectroradiometer spectral reflectance, *J. Geophys. Res.*, *112*, D13211, doi:10.1029/2006JD007811.

Misra, A., S. N. Tripathi, D. S. Kaul, and E. J. Welton (2012), Study of MPLNET-derived aerosol climatology over Kanpur, India, and validation of CALIPSO level 2 version 3 backscatter and extinction products, *J. Atmos. Oceanic Technol.*, *29*, 1285–1294.

Novakov, T., M. O. Andreae, R. Gabriel, T. W. Kirchstetter, O. L. Mayol-Bracero, and V. Ramanathan (2000), Origin of carbonaceous aerosols over the tropical Indian Ocean: Biomass burning or fossil fuels, *Geophys. Res. Lett.*, *27*, 4061–4064, doi:10.1029/2000GL011759.

O'Neill, N. T., T. F. Eck, B. N. Holben, A. Smirnov, O. Dubovik, and A. Royer (2001), Bimodal size distribution influences on the variation of Ångström derivatives in spectral and optical depth space, *J. Geophys. Res.*, *106*(D9), 9787–9806, doi:10.1029/2000JD900245.

O'Neill, N. T., T. F. Eck, A. Smirnov, B. N. Holben, and S. Thulasiraman (2003), Spectral discrimination of coarse and fine mode optical depth, *J. Geophys. Res.*, *108*(D17), 4559, doi:10.1029/2002JD002975.

Pandithurai, G., S. Dipu, K. K. Dani, S. Tiwari, D. S. Bisht, P. C. S. Devara, and R. T. Pinker (2008), Aerosol radiative forcing during dust events over New Delhi, India, *J. Geophys. Res.*, *113*, D13209, doi:10.1029/2008JD009804.

Pathak, B., G. Kalita, K. Bhuyan, P. K. Bhuyan, and K. K. Moorthy (2010), Aerosol temporal characteristics and its impact on shortwave radiative forcing at a location in the northeast of India, *J. Geophys. Res.*, *115*, D19204, doi:10.1029/2009JD013462.

Podgorny, I. A., W. Conant, V. Ramanathan, and S. K. Satheesh (2000), Aerosol modulation of atmospheric and surface solar heating over the tropical Indian Ocean, *Tellus B*, *52*, 947–958.

Prasad, A. K., and R. P. Singh (2007), Changes in aerosol parameters during major dust storm events (2001–2005) over the Indo-Gangetic Plains using AERONET and MODIS data, *J. Geophys. Res.*, *112*, D09208, doi:10.1029/2006JD007778.

Prasad, A. K., S. Singh, S. S. Chauhan, M. K. Srivastava, R. P. Singh, and R. Singh (2007), Aerosol radiative forcing over the Indo-Gangetic plains during major dust storms, *Atmos. Environ.*, *41*(29), 6289–6301, doi:10.1016/j.atmosenv.2007.03.060.

Ram, K., M. M. Sarin, and P. Hegde (2010), Long-term record of aerosol optical properties and chemical composition from a high-altitude site (Manora Peak) in Central Himalaya, *Atmos. Chem. Phys.*, *10*, 11,791–11,803, doi:10.5194/acp-10-11791-2010.

Ramachandran, S., and S. Kedia (2010), Black carbon aerosols over an urban region: Radiative forcing and climate impact, *J. Geophys. Res.*, *115*, D10202, doi:10.1029/2009JD013560.

Remer, L. A., et al. (2008), Global aerosol climatology from the MODIS satellite sensors, *J. Geophys. Res.*, *113*, D14S07, doi:10.1029/2007JD009661.

Ricchiazzi, P., S. Yang, C. Gautier, and D. Sowle (1998), SBDART: A research and software tool for plane-parallel radiative transfer in the Earth's atmosphere, *Bull. Am. Meteorol. Soc.*, *79*, 2101–2114.

Russell, P. B., R. W. Bergstrom, Y. Shinozuka, A. D. Clarke, P. F. DeCarlo, J. L. Jimenez, J. M. Livingston, J. Redemann, O. Dubovik, and A. Strawa (2010), Absorption Ångström Exponent in AERONET and related data as an indicator of aerosol composition, *Atmos. Chem. Phys.*, *10*, 1155–1169, doi:10.5194/acp-10-1155-2010.

Satheesh, S. K., and V. Ramanathan (2000), Large differences in tropical aerosol forcing at the top of the atmosphere and Earth's surface, *Nature*, *405*, 60–63.

Satheesh, S. K., V. Vinoj, and K. Krishna Moorthy (2010), Radiative effects of aerosols at an urban location in southern India: Observations versus model, *Atmos. Environ.*, *44*, 5295–5304, doi:10.1016/j.atmosenv.2010.07.020.

Singh, R. P., S. Dey, S. N. Tripathi, and V. Tare (2004), Variability of aerosol parameters over Kanpur, northern India, *J. Geophys. Res.*, *109*, D23206, doi:10.1029/2004JD004966.

Singh, S., K. Soni, T. Bano, R. S. Tanwar, S. Nath, and B. C. Arya (2010), Clear-sky direct aerosol radiative forcing variations over mega-city Delhi, *Ann. Geophys.*, *28*, 1157–1166, doi:10.5194/angeo-28-1157-2010.

Smirnov, A., B. N. Holben, T. F. Eck, O. Dubovik, and I. Slutsker (2000), Cloud screening and quality control algorithms for the AERONET database, *Remote Sens. Environ.*, *73*(3), 337–349.

Smirnov, A., B. N. Holben, A. Lyapustin, I. Slutsker, and T. F. Eck (2004), AERONET processing algorithms refinement, paper presented at AERONET Workshop, El Arenosillo, Spain, 10–14 May.

Soni, K., S. Singh, T. Bano, R. S. Tanwar, S. Nath, and B. C. Arya (2010), Variations in single scattering albedo and Ångström absorption exponent during different seasons at Delhi, India, *Atmos. Environ.*, *44*, 4355–4363.

Srivastava, A. K., S. Tiwari, P. C. S. Devara, D. S. Bisht, M. K. Srivastava, S. N. Tripathi, P. Goloub, and B. N. Holben (2011), Pre-monsoon aerosol characteristics over the Indo-Gangetic Basin: Implications to climate impact, *Ann. Geophys.*, *29*, 789–804.

Srivastava, A. K., S. N. Tripathi, S. Dey, V. P. Kanawade, and S. Tiwari (2012), Inferring aerosol types over the Indo-Gangetic basin from ground based sunphotometer measurements, *Atmos. Res.*, *109*, 64–75, doi:10.1016/j.atmosres.2012.02.010.

Tripathi, S. N., S. Dey, V. Tare, S. K. Satheesh, S. Lal, and S. Venkataramani (2005), Enhanced layer of black carbon in a north Indian industrial city, *Geophys. Res. Lett.*, *32*, L12802, doi:10.1029/2005GL022564.

Tripathi, S. N., A. K. Srivastva, S. Dey, S. K. Satheesh, and K. Krishnamurthy (2007), The vertical profile of atmospheric heating rate of black carbon aerosols at Kanpur in northern India, *Atmos. Environ.*, *41*(32), 6909–6915.

Uno, I., K. Eguchi, K. Yumimoto, T. Takemura, A. Shimizu, M. Uematsu, Z. Liu, Z. Wang, Y. Hara, and N. Sugimoto (2009), Asian dust transported one full circuit around the globe, *Nat. Geosci.*, *2*, 557–560.

Winker, D. M., W. H. Hunt, and M. J. McGill (2007), Initial performance assessment of CALIOP, *Geophys. Res. Lett.*, *34*, L19803, doi:10.1029/2007GL030135.